sequentially operating enzymes. For instance, the enzymes citrate synthase (CS) and malate dehydrogenase (MDH) have been covalently coupled to a Sepharose matrix and the kinetics of the sequential reaction was investigated [41]. The results showed a reduction in the lag time of the overall enzyme reaction and a higher steady-state rate compared to a solution of the free enzymes. To study the possible effects of the immobilizing matrix material on the enzymes, they were also chemically cross-linked to each other in solution, yielding soluble enzyme conjugates [42].However, these conjugates did not exhibit any kinetic advantages compared to a system with free enzymes except when precipitated with PEG. This might be a result of the effects caused by the cross-linking method which in general is difficult to control. In another study, Spivey and co-workers were able to demonstrate intermediate substrate (OAA) sequestration in the overall reaction of malate to citrate using a PEG co-precipitated solid state preparation of pig CS and MDH [43]. It has been proposed that a better model for the study of proximity effects would be to use a system consisting of sequential enzymes fused by molecular biological techniques [44]. A number of bi-enzymatic fusion proteins which catalyze sequential reactions have been constructed [36,45]. They have shown kinetic benefits for the overall reaction, such as shorter lag times (transient times) and an apparent sequestering of the intermediate by the fusion system when compared to the free enzymes in the presence of an enzyme trap for the intermediate metabolite [35,36,45]. Substrate channelling occurs because of close proximity (40–60 Å) of the active sites of the interacting enzymes [30]. Analysis of the energy minimized average model of the EhPGDH-PSAT enzyme complex suggests that active sites of the two enzymes are closely associated (Fig. 5B). Furthermore the EhPGDH-PSAT complex showed as Km of 100 ± 10 μM for 3-PGA which was significantly lower than that observed for the individual PGDH enzyme (225 ± 7 μM). The results suggest that the product of PDGH catalyzed reaction is been taken up by its interacting partner PSAT which in turn shifts the reaction equilibrium in forward direction. 3-Phosphoserine, the final product of the enzyme complex catalyzed reaction can be taken up by phosphoserine phosphatase (PSP) or cysteine synthase (CS) in their respective committed reactions for the formation of L-serine or L-cysteine [46].

4. Conclusions

E. histolytica phosphoglycerate dehydrogenase (EhPGDH) specifically interacts with phosphoserine aminotransferase (EhPSAT) under *in vitro* conditions. The protein–protein complex has a 1:1 stoichiometry with a dissociation constant of 3.453×10^{-7} M. Ionic interactions play a significant role in complex stability. The two domains Nbd and Sbd of EhPGDH are independent folding/unfolding units. The Nbd specifically forms the binding interface of the complex with the PLP-binding domain of EhPSAT. The active sites of the two partners of the complex are proximally located which leads to sequestering of the reaction intermediates leading to substrate channelling in the complex.

Conflict of interest

None declared.

Acknowledgements

In acknowledgement of his intellectual skills that guided this work VM, AK, VA, KYJZ and TN dedicate this paper to the memory of our co-author, Vinod Bhakuni. We thank Md. Sohail Akhtar for useful discussions and/or comments on the manuscript. We thank Swati Tyagi for laboratory help. VM is grateful to CSIR New Delhi for financial assistance. This is communication number 8214 from CSIR–CDRI.

Appendix. Supplementary material

Supplementary data related to this article can be found online at doi:10.1016/j.biochi.2012.02.028.

References

[1] P.A. Srere, J. Ovadi, Enzyme–enzyme interactions and their metabolic role, FEBS. Lett. 268 (1990) 360–364.
[2] P.A. Srere, Complexes of sequential metabolic enzymes, Ann. Rev. Biochem. 56 (1987) 89–124.
[3] J.B. Robinson Jr., P.A. Srere, Organization of Krebs tricarboxylic acid cycle enzymes, Biochem. Med. 33 (1985) 149–157.
[4] X. Huang, H.M. Holden, F.M. Raushel, Channeling of substrates and intermediates in enzyme-catalyzed reactions, Annu. Rev. Biochem. 70 (2001) 149–180.
[5] B. Sumegi, A.D. Sherry, C.R. Malloy, C. Evans, P.A. Srere, Is there tight channelling in the tricarboxylic acid cycle metabolon? Biochem. Soc. Trans. 19 (1991) 1002–1005.
[6] I. Morgunov, P.A. Srere, Interaction between citrate synthase and malate dehydrogenase. Substrate channeling of oxaloacetate, J. Biol. Chem. 273 (1998) 29540–29544.
[7] C. Velot, S. Lebreton, I. Morgunov, K.C. Usher, P.A. Srere, Metabolic effects of mislocalized mitochondrial and peroxisomal citrate synthases in yeast *Saccharomyces cerevisiae*, Biochemistry 38 (1999) 16195–16204.
[8] G. Igor, I. Morgunov, V. Svetlana, The binding of citrate synthase and malate dehydrogenase with the inner mitochondrial membrane, J. Biomol. Struct. Dyn. 26 (2009) 870–871.
[9] V. Ali, T. Hashimoto, Y. Shigeta, T. Nozaki, Molecular and biochemical characterization of D-phosphoglycerate dehydrogenase from *Entamoeba histolytica*. A unique enteric protozoan parasite that possesses both phosphorylated and nonphosphorylated serine metabolic pathways, FEBS. J. 271 (2004) 2670–2681.
[10] V. Mishra, A. Kumar, V. Ali, T. Nozaki, K.Y. Zhang, V. Bhakuni, Glu-108 is essential for subunit assembly and dimer stability of D-phosphoglycerate dehydrogenase from *Entamoeba histolytica*, Mol. Biochem. Parasitol. (2011) Oct 23 Epub ahead of print.
[11] V. Mishra, V. Ali, T. Nozaki, V. Bhakuni, *Entamoeba histolytica* phosphoserine aminotransferase (EhPSAT): insights into the structure–function relationship, BMC, Res. Notes 3 (2010) 52.
[12] V. Mishra, A. Kumar, V. Ali, T. Nozaki, K.Y. Zhang, V. Bhakuni, Role of conserved active site tryptophan-101 in functional activity and stability of phosphoserine aminotransferase from an enteric human parasite, Amino Acids. (2011) Oct29 Epub ahead of print.
[13] A. Sali, T.L. Blundell, Comparative protein modelling by satisfaction of spatial restraints, J. Mol. Biol. 234 (1993) 779–815.
[14] D. Schneidman-Duhovny, Y. Inbar, R. Nussinov, H.J. Wolfson, PatchDock and SymmDock: servers for rigid and symmetric docking, Nucleic Acids Res. 33 (2005) W363–W367.
[15] J.J. Gray, S. Moughon, C. Wang, O. Schueler-Furman, B. Kuhlman, C.A. Rohl, D. Baker, Protein–protein docking with simultaneous optimization of rigid-body displacement and side-chain conformations, J. Mol. Biol. 331 (2003) 281–299.
[16] K.T. Simons, C. Kooperberg, E. Huang, D. Baker, Assembly of protein tertiary structures from fragments with similar local sequences using simulated annealing and Bayesian scoring functions, J. Mol. Biol. 268 (1997) 209–225.
[17] K.T. Simons, I. Ruczinski, C. Kooperberg, B.A. . Fox, C. Bystroff, D. Baker, Improved recognition of native-like protein structures using a combination of sequence-dependent and sequence-independent features of proteins, Proteins 34 (1999) 82–95.
[18] J.J. Gray, S.E. Moughon, T. Kortemme, O. Schueler-Furman, K.M. Misura, A.V. Morozov, D. Baker, Protein-protein docking predictions for the CAPRI experiment, Proteins 52 (2003) 118–122.
[19] T. Lazaridis, M. Karplus, Effective energy function for proteins in solution, Proteins 35 (1999) 133–152.
[20] T. Kortemme, A.V. Morozov, D. Baker, An orientation-dependent hydrogen bonding potential improves prediction of specificity and structure for proteins and protein-protein complexes, J. Mol. Biol. 326 (2003) 1239–1259.
[21] D.Y. Tom Darden, Lee Pedersen, Particle mesh Ewald: an N-log(N) method for Ewald sums in large systems, J. Chem. Phys. 98 (1993) 10089–10092.
[22] J.P. Ryckaert, G. Ciccotti, H.J.C. Berendsen, Numerical-integration of Cartesian Equations of motion of a system with constraints – molecular-dynamics of N-alkanes, J. Comput. Phys. 23 (1977) 327–341.
[23] D.A. Case, T.E. Cheatham 3rd, T. Darden, H. Gohlke, R. Luo, K.M. Merz Jr., A. Onufriev, C. Simmerling, B. Wang, R.J. Woods, The Amber biomolecular simulation programs, J. Comput. Chem. 26 (2005) 1668–1688.

[24] M.A. Andrade, P. Chacon, J.J. Merelo, F. Moran, Evaluation of secondary structure of proteins from UV circular dichroism spectra using an unsupervised learning neural network, Protein Eng. 6 (1993) 383–390.
[25] J.R. Lakowicz, Principles of Fluorescence Spectroscopy, Springer, New York, 2006.
[26] W.G. Hearl, J.E. Churchich, Interactions between 4-aminobutyrate aminotransferase and succinic semialdehyde dehydrogenase, two mitochondrial enzymes, J. Biol. Chem. 259 (1984) 11459–11463.
[27] R.A. Laskowski, D.S. Moss, J.M. Thornton, PROCHECK: a program to check the stereochemical quality of protein structures, J. Appl. Cryst 26 (1993) 283–291.
[28] J. Ovadi, P.A. Srere, Metabolic consequences of enzyme interactions, Cell. Biochem. Funct. 14 (1996) 249–258.
[29] J. Ovadi, P.A. Srere, Macromolecular compartmentation and channeling, Int. Rev. Cytol. 192 (2000) 255–280.
[30] H.O. Spivey, J. Ovadi, Substrate channeling, Methods 19 (1999) 306–321.
[31] S. Shallom, K. Zhang, L. Jiang, P.K. Rathod, Essential protein-protein interactions between *Plasmodium falciparum* thymidylate synthase and dihydrofolate reductase domains, J. Biol. Chem. 274 (1999) 37781–37786.
[32] P. Tompa, J. Batke, J. Ovadi, G.R. Welch, P.A. Srere, Quantitation of the interaction between citrate synthase and malate dehydrogenase, J. Biol. Chem. 262 (1987) 6089–6092.
[33] M.M. Islam, M. Nautiyal, R.M. Wynn, J.A. Mobley, D.T. Chuang, S.M. Hutson, Branched-chain amino acid metabolon: interaction of glutamate dehydrogenase with the mitochondrial branched-chain aminotransferase (BCATm), J. Biol. Chem. 285 (2010) 265–276.
[34] L.A. Nogaj, S.I. Beale, Physical and kinetic interactions between glutamyl-tRNA reductase and glutamate-1-semialdehyde aminotransferase of *Chlamydomonas reinhardtii*, J.Biol. Chem. 280 (2005) 24301–24307.
[35] L. Bulow, Characterization of an artificial bifunctional enzyme, beta-galactosidase/galactokinase, prepared by gene fusion, FEBS J. 163 (1987) 443–448.
[36] P. Ljungcrantz, H. Carlsson, M.O. Mansson, P. Buckel, K. Mosbach, L. Bulow, Construction of an artificial bifunctional enzyme, beta-galactosidase/galactose dehydrogenase, exhibiting efficient galactose channeling, Biochemistry 28 (1989) 8786–8792.
[37] B. Sumegi, H.F. Gilbert, P.A. Srere, Interaction between citrate synthase and thiolase, J. Biol. Chem. 260 (1985) 188–190.
[38] S.J. Barnes, P.D. Weitzman, Organization of citric acid cycle enzymes into a multienzyme cluster, FEBS. Lett. 201 (1986) 267–270.
[39] J.B. Robinson Jr., L. Inman, B. Sumegi, P.A. Srere, Further characterization of the Krebs tricarboxylic acid cycle metabolon, J. Biol. Chem. 262 (1987) 1786–1790.
[40] B. Sumegi, Z. Porpaczy, M.T. McCammon, A.D. Sherry, C.R. Malloy, P.A. Srere, Regulatory consequences of organization of citric acid cycle enzymes, Curr. Top. Cell. Reg. 33 (1992) 249–260.
[41] P.A. Srere, B. Mattiasson, K. Mosbach, An immobilized three-enzyme system: a model for microenvironmental compartmentation in mitochondria, Proc. Natl. Acad. Sci. 70 (1973) 2534–2538.
[42] A.C. Koch-Schmidt, K. Mosbach, Studies on conformation of soluble and immobilized enzymes using differential scanning calorimetry. 2. Specific activity and thermal stability of enzymes bound weakly and strongly to Sepharose CL 4B, Biochemistry 16 (1977) 2105–2109.
[43] A. Datta, J.M. Merz, H.O. Spivey, Substrate channeling of oxalacetate in solid-state complexes of malate dehydrogenase and citrate synthase, J. Biol. Chem. 260 (1985) 15008–15012.
[44] L. Bulow, K. Mosbach, Multienzyme systems obtained by gene fusion, Trends Biotechnol 9 (1991) 226–231.
[45] L. Bulow, K. Mosbach, Preparation of bifunctional enzyme complexes by fusion of two genes, Ann. NY. Aca. Sci. 501 (1987) 44–49.
[46] G.D. Westrop, G. Goodall, J.C. Mottram, G.H. Coombs, Cysteine biosynthesis in *Trichomonas vaginalis* involves cysteine synthase utilizing O-phosphoserine, J. Biol. Chem. 281 (2006) 25062–25075.

OPEN ACCESS Freely available online

PLOS | NEGLECTED TROPICAL DISEASES

Dramatic Increase in Glycerol Biosynthesis upon Oxidative Stress in the Anaerobic Protozoan Parasite *Entamoeba histolytica*

Afzal Husain[1,2¤], Dan Sato[3], Ghulam Jeelani[1,4], Tomoyoshi Soga[3], Tomoyoshi Nozaki[1,5*]

1 Department of Parasitology, National Institute of Infectious Diseases, Tokyo, Japan, **2** Department of Parasitology, Gunma University Graduate School of Medicine, Maebashi, Japan, **3** Institute for Advanced Biosciences, Keio University, Tsuruoka, Japan, **4** Department of Biochemistry and Integrative Medical Biology, School of Medicine, Keio University, Tokyo, Japan, **5** Graduate School of Life and Environmental Sciences, University of Tsukuba, Tsukuba, Japan

Abstract

Entamoeba histolytica, a microaerophilic enteric protozoan parasite, causes amebic colitis and extra intestinal abscesses in millions of inhabitants of endemic areas. Trophozoites of *E. histolytica* are exposed to a variety of reactive oxygen and nitrogen species during infection. Since *E. histolytica* lacks key components of canonical eukaryotic anti-oxidative defense systems, such as catalase and glutathione system, alternative not-yet-identified anti-oxidative defense strategies have been postulated to be operating in *E. histolytica*. In the present study, we investigated global metabolic responses in *E. histolytica* in response to H_2O_2- and paraquat-mediated oxidative stress by measuring charged metabolites on capillary electrophoresis and time-of-flight mass spectrometry. We found that oxidative stress caused drastic modulation of metabolites involved in glycolysis, chitin biosynthesis, and nucleotide and amino acid metabolism. Oxidative stress resulted in the inhibition of glycolysis as a result of inactivation of several key enzymes, leading to the redirection of metabolic flux towards glycerol production, chitin biosynthesis, and the non-oxidative branch of the pentose phosphate pathway. As a result of the repression of glycolysis as evidenced by the accumulation of glycolytic intermediates upstream of pyruvate, and reduced ethanol production, the levels of nucleoside triphosphates were decreased. We also showed for the first time the presence of functional glycerol biosynthetic pathway in *E. histolytica* as demonstrated by the increased production of glycerol 3-phosphate and glycerol upon oxidative stress. We proposed the significance of the glycerol biosynthetic pathway as a metabolic anti-oxidative defense system in *E. histolytica*.

Citation: Husain A, Sato D, Jeelani G, Soga T, Nozaki T (2012) Dramatic Increase in Glycerol Biosynthesis upon Oxidative Stress in the Anaerobic Protozoan Parasite *Entamoeba histolytica*. PLoS Negl Trop Dis 6(9): e1831. doi:10.1371/journal.pntd.0001831

Editor: Kiyoshi Kita, University of Tokyo, Japan

Received March 29, 2012; **Accepted** August 10, 2012; **Published** September 27, 2012

Funding: This work was supported by a Grant-in-Aid for Scientific Research from the Ministry of Education, Culture, Sports, Science and Technology (MEXT) of Japan to T.N. (23117001, 23117005, 23390099), and to D.S. (20590429), a Grant-in-Aid on Bilateral Programs of Joint Research Projects and Seminars from Japan Society for the Promotion of Science, a Grant-in-Aid on Strategic International Research Cooperative Program from Japan Science and Technology Agency, a grant for research on emerging and re-emerging infectious diseases from the Ministry of Health, Labour and Welfare of Japan (H23-Shinko-ippan-014) to T.N., a grant for research to promote the development of anti-AIDS pharmaceuticals from the Japan Health Sciences Foundation (KHA1101) to T.N. and by Global COE Program (Global COE for Human Metabolomic Systems Biology) from MEXT, Japan to G.J. and T.N.. The funders had no role in study design, data collection and analysis, decision to publish, or preparation of the manuscript.

Competing Interests: The authors have declared that no competing interests exist.

* E-mail: nozaki@nih.go.jp

¤ Current address: Department of Immunology and Genomic Medicine, Graduate School of Medicine, Kyoto University Kyoto, Japan

Introduction

Organisms are exposed to a variety of reactive oxygen and nitrogen species (ROS and RNS) that cause damage to key biomolecules such as proteins, lipids and DNA, and lead to cellular dysfunction [1–3]. In many cases, oxidative stress also induces genetic programs such as apoptosis, which ultimately leads to cell death [3–6]. In order to protect themselves against these oxidative damages, cells utilize effective defense mechanisms including antioxidant enzymes and free radical scavengers [7]. It is now well established that most microbial and higher eukaryotic cells have the ability to cope with oxidative stress by altering global expression of antioxidants and other metabolic enzyme encoding genes at transcriptional and post-transcriptional levels. However, it is becoming increasingly acceptable that post-translational mechanisms are also important players of cellular responses to oxidative stress. For instance, it has recently been shown that upon oxidative stress, metabolic flux is redirected from glycolysis to the pentose phosphate pathway to synthesize reductant for antioxidant metabolism [8].

Entamoeba histolytica is a protozoan parasite that causes dysentery and extra intestinal abscesses in millions of inhabitants of endemic areas [9]. *E. histolytica* trophozoites are microaerophilic, and have been shown to consume oxygen, and tolerate low levels of oxygen pressure [10]. In addition, they are also exposed to various reactive oxygen or nitrogen species (ROS and RNS) during tissue invasion, colonization, and extra intestinal propagation [9,11]. *E. histolytica* lacks most of the components, such as catalase, reduced glutathione, and the glutathione-recycling enzymes [12–14], involved in the usual antioxidant defense mechanisms in aerobic organisms. *E. histolytica* also lacks glucose 6-phosphate dehydrogenase (G6PD), and thus functional pentose phosphate pathway (PPP) is absent [12]. However, the genome of *E. histolytica* encodes several proteins such as peroxiredoxin, superoxide dismutase,

Author Summary

During the course of infection, trophozoites of *E. histolytica* need to cope with the oxidative stress in order to survive under the oxidative environment of its host. As a result of the absence of the key eukaryotic anti-oxidative defense system, it needs to employ novel defense strategies. Several studies such as transcriptomic profiling of trophozoites exposed to oxidative stress, and biochemical and functional analysis of individual proteins has been done in the past. Since, oxidative stress damages several metabolic enzymes, and modulate expression of many genes, it is important to analyze the detailed metabolomic response of *E. histolytica* upon oxidative stress to understand the role of metabolism in combating oxidative stress. In the present study, we demonstrated that oxidative stress causes glycolytic inhibition and redirection of metabolic flux towards glycerol production, chitin biosynthesis, and the non-oxidative branch of the pentose phosphate pathway.

rubrerythrin, hybrid-cluster protein, and flavo-di-iron proteins for detoxification of ROS and RNS [12,15,16]. In addition, *E. histolytica* also possesses a cryptic pyridine nucleotide transhydrogenase, which utilizes the electrochemical proton gradient across the membrane to drive NADPH synthesis from NADH [17,18].

The precise nature of the molecular response to oxidative stress in *E. histolytica* is poorly understood. Several genes have shown to be differentially expressed in *E. histolytica* subjected to oxidative or nitrosative stress [19]. However, the specific regulatory elements of this transcriptomic response are yet to be uncovered. It has been shown that in bacteria and yeast, the expression of genes involved in antioxidative defense mechanisms is partially induced upon oxidative stress [20,21]. However, like most eukaryotic cells, the transcription of genes encoding enzymes capable of neutralizing ROS and RNS is generally not increased in *E. histolytica* subjected to oxidative stress [19]. In yeast and bacteria, post transcriptional and post translational studies have recently demonstrated that a large number of metabolic enzymes are targeted by oxidative stress that led to redirection of metabolic flux [8]. What little is known in *E. histolytica* relates to oxidative stress-dependent inactivation of some enzymes involved in central energy metabolism [22]. However, it remains unknown how *E. histolytica* and other organisms that lack fully functional PPP such as *Trichomonas* and *Giardia* [23,24] respond to oxidative stress at the metabolic level.

In order to get insight into the dynamics of metabolic changes employed either to bypass damaged enzymes or to support adaptive responses to cope up with oxidative stress, we undertook detailed metabolomic study of *E. histolytica* upon oxidative stress. We employed capillary electrophoresis time-of-flight mass spectrometry (CE-TOFMS) [25–27] to simultaneously detect and quantify hundreds of intermediary metabolites of primary metabolism. The major advantages of CE-TOFMS analysis include its extremely high resolution and ability to simultaneously quantify a variety of charged low-molecular weight compounds [25–27]. In the present study, we highlight several unanticipated oxidative stress-mediated metabolomic changes, and discuss their relevance in relation to oxidative stress in *E. histolytica*. In addition to metabolomic analysis, the activities of several enzymes that are of potential importance in regulating observed metabolomic changes are evaluated. The obtained data are discussed in terms of the correlations between the metabolome and posttranslational inactivation of key metabolic enzymes.

Materials and Methods

Chemicals and reagents

All chemicals of analytical grade were purchased from either Wako (Tokyo, Japan) or Sigma-Aldrich (Tokyo, Japan) unless otherwise mentioned. 2′, 7′-Dichlorodihydrofluorescein di-acetate (2′, 7′-DCF-DA) was purchased from Invitrogen. Stock solutions of metabolite standards (1–100 mmol/L) for CE-MS analysis were prepared in either Milli-Q water, 0.1 mol/L HCl, or 0.1 mol/L NaOH. A mixed solution of the standards was prepared by diluting stock solutions with Milli-Q water immediately before CE-TOFMS analysis.

Microorganisms and cultivation

Trophozoites of the *E. histolytica* clonal strain HM-1: IMSS cl 6 were maintained axenically in Diamond's BI-S-33 medium at 35.5°C, as described previously [28,29]. Trophozoites were harvested in the late-logarithmic growth phase 2–3 days after the inoculation of medium with one-thirtieth to one-twelfth of the total culture volume.

Induction of oxidative stress and metabolite extraction

E. histolytica trophozoites were cultivated in standard BI-S-33 medium until late logarithmic phase in 36 ml culture flaks, and then culture medium was replaced with fresh and warm culture medium. To induce oxidative stress, paraquat (PQ) or H_2O_2 were added to the final concentration of 1 or 0.4 mM, respectively, and culture was continued for next 1, 3, 6, or 12 h. Intracellular metabolites were extracted as previously described with some modifications [30,31]. Approximately 1.5×10^6 trophozoites from each condition were harvested and immediately suspended in 1.6 ml of −75°C methanol to quench metabolic activity. To ensure that experimental artifacts such as ion suppression did not lead to misinterpretation of metabolite levels, internal standards, 2-(*N*-morpholino) ethanesulfonic acid, methionine sulfone, and D-camphor-10-sulfonic acid were added to every sample. The samples were then sonicated for 30 second and mixed with 1.6 ml of chloroform, and 640 µl of deionized water. After vortexing, the mixture was centrifuged at 4,600× *g* at 4°C for 5 min. The aqueous layer (1.6 ml) was filtrated using an Amicon Ultrafree-MC ultrafilter (Millipore Co., Massachusetts, USA) and centrifuged at 9,100× *g* at 4°C for approximately 2 h. The filtrate was dried and preserved at −80°C until mass spectrometric analysis [30,32]. Prior to the analysis, metabolic extracts was dissolved in 20 µl of de-ionized water containing reference compounds (200 µmol/L each of 3-aminopyrrolidine and trimesic acid).

Instrumentation and capillary electrophoresis-time-of-flight mass spectrometry (CE-TOFMS) conditions

CE-TOFMS was performed using an Agilent CE Capillary Electrophoresis System equipped with an Agilent 6210 Time-of-Flight mass spectrometer, Agilent 1100 isocratic HPLC pump, Agilent G1603A CE-MS adapter kit, and Agilent G1607A CE-ESI-MS sprayer kit (Agilent Technologies, Waldbronn, Germany). The system was controlled by Agilent G2201AA ChemStation software for CE. Data acquisition was performed by Analyst QS software for Agilent TOF (Applied Biosystems, CA, USA; MDS Sciex, Ontario, Canada).

CE-TOFMS conditions for cationic metabolite analysis

Cationic metabolites were separated in a fused-silica capillary (50 µm i.d.×100 cm total length) filled with 1 mol/L formic acid as the reference electrolyte [33]. Sample solution (~3 nL) was injected at 50 mbar for 3 s, and a positive voltage of 30 kV was applied. The capillary and sample trays were maintained at 20°C

and below 5°C, respectively. Sheath liquid composed of methanol/water (50% v/v) that contained 0.1 μmol/L hexakis (2,2-difluoroethoxy) phosphazene was delivered at 10 μL/min. ESI-TOFMS was operated in the positive ion mode. The capillary voltage was set at 4 kV and a flow rate of nitrogen gas (heater temperature 300°C) was set at 10 psig. For TOFMS, the fragmenter voltage, skimmer voltage, and octapole radio frequency voltage (Oct RFV) were set at 75, 50, and 125 V, respectively. An automatic recalibration function was performed using two reference masses of reference standards; protonated ^{13}C methanol dimer (m/z 66.063061) and protonated hexakis (2,2-difluoroethoxy) phosphazene (m/z 622.028963), which provided the lock mass for exact mass measurements. Exact mass data were acquired at the rate of 1.5 cycles/s over a 50 to 1,000 m/z range.

CE-TOFMS conditions for anionic metabolite analysis

Anionic metabolites were separated in a cationic-polymer–coated COSMO(+) capillary (50 μm i.d.×110 cm) (Nacalai Tesque) filled with 50 mmol/L ammonium acetate solution (pH 8.5) as the reference electrolyte [34,35]. Sample solution (~30 nL) was injected at 50 mbar for 30 s and a negative voltage of −30 kV was applied. Ammonium acetate (5 mmol/L) in 50% methanol/water (50% v/v) that contained 0.1 μmol/L hexakis (2,2-difluoroethoxy) phosphazene was delivered as sheath liquid at 10 μL/min. ESI-TOFMS was operated in the negative ion mode. The capillary voltage was set at 3.5 kV. For TOFMS, the fragmenter voltage, skimmer voltage, and Oct RFV were set at 100, 50, and 200 V, respectively [35]. An automatic recalibration function was performed using two reference masses of reference standards: deprotonated ^{13}C acetate dimer (m/z 120.038339) and acetate adduct of hexakis (2,2-difluoroethoxy) phosphazene (m/z 680.035541). The other conditions were identical to those used for the cationic metabolome analysis.

CE-TOFMS data processing

Raw data were processed using the in-house software Masterhands [36]. The overall data processing flow consisted of the following steps: noise-filtering, baseline-removal, migration time correction, peak detection, and integration of peak area from a 0.02 m/z-wide slice of the electropherograms. This process resembled the strategies employed in widely used data processing software for LC-MS and GC-MS data analysis, such as MassHunter (Agilent Technologies) and XCMS [37]. Subsequently, accurate m/z values for each peak were calculated by Gaussian curve fitting in the m/z domain, and migration times were normalized using alignment algorithms based on dynamic programming [25,38]. All target metabolites were identified by matching their m/z values and normalized migration times with those of standard compounds in the in-house library.

Assay of enzymatic activities

In order to assay activities of various enzymes of central energy metabolism, *E. histolytica* trophozoites were exposed to PQ as described above. Trophozoites were harvested by chilling on ice, centrifuging at 450 g, and washing twice with NaCl/Pi at pH 7.4. Trophozoites were then lysed in NaCl/Pi (pH 7.0) by freezing–thawing. The insoluble materials were eliminated by centrifugation at 15 000× g for 10 min. The activities of several glycolytic enzymes in the soluble fraction were determined as described previously [22].

Quantitation of Reactive Oxygen Species

Fluorescence spectrophotometry was used to measure the production of intracellular reactive oxygen species using 2′, 7′-DCF-DA as a probe as previously described [30]. Briefly, untreated or 1 mM PQ treated *E. histolytica* trophozoites were washed in PBS, and 5.0×10^5 cells were then incubated in 1 ml of PBS containing 20 μM of 2′, 7′-DCF-DA for 30 min at 35.5°C in the dark. The intensity of fluorescence was immediately read at excitation and emission wavelengths of 492 and 519 nm, respectively.

Glycerol, ethanol and acetate quantitation

To estimate the production of glycerol, ethanol or acetate, approximately 10^7 normally cultured or stressed trophozoites (1 mM PQ for 12 h) were suspended in 1.0 mL of NaCl/Pi (117 mM NaCl, 2.3 mM KCl, 8.5 mM Na_2HPO_4, 1.7 mM KH2PO4; pH 7.4) containing 1% glucose (w/v), and incubated in a water bath at 35.5°C. After 30 min, the cells were quickly harvested by centrifugation at 500× g for 5 min. Supernatants were used for the estimation of ethanol, acetate and glycerol. The cellular pellets were extracted with perchloric acid, as described earlier and used for the estimation of intracellular glycerol. Ethanol and glycerol were determined using ethanol or glycerol estimation kits from Biovision (Mountain View, CA). Acetate was estimated by using acetate kinase through the coupling reaction of this enzyme with pyruvate kinase, and lactate dehydrogenase [30]. Acetate kinase generates ADP and acetyl-phosphate from acetate and ATP. The ADP production was coupled with the oxidation of NADH ($\varepsilon_{340} = 6.22\ mM^{-1}\ cm^{-1}$) through pyruvate kinase and lactate dehydrogenase. The standard reaction mixture contained 50 mM of Tris-Cl, 3 units each of acetate kinase, pyruvate kinase and lactate dehydrogenase, 0.5 mM ATP, 0.3 mM NADH, and 0.4 mM phosphoenolpyruvate (PEP). Reactions were initiated by the addition of supernatant containing acetate, and optical absorbance was read at 340 nm on a Shimadzu spectrophotometer.

Results and Discussion

Oxidative stress causes drastic changes in the metabolome of *E. histolytica*

In order to study metabolomic responses of *E. histolytica* upon oxidative stress, we exposed amebic trophozoites to hydrogen peroxide (H_2O_2) or paraquat (PQ), which are widely used to study oxidative stress in various organisms. Peroxide stress was generated by directly adding H_2O_2 to a desired concentration, whereas superoxide stress was generated indirectly during metabolism of exogenously added PQ [Fig. 1C]. In order to identify conditions to monitor short- to long-term (~12 h) responses, in which trophozoites were stressed, and still viable, we estimated the survival of trophozoites upon treatment with varying concentrations of PQ (0.25–8.0 mM) or H_2O_2 (0.2–6.4 mM) for 12 h. Trophozoites exposed to 1 mM of PQ or 400 μM of H_2O_2 for 12 h showed a viability of ≥90%, while trophozoites exposed to higher concentrations showed lesser viability (Fig. 1, A and B). Thus, we chose 1 mM of PQ or 400 μM of H_2O_2, and exposed trophozoites for 1, 3, 6, or 12 h to these oxidants, and compared the metabolome with that of untreated trophozoites. Approximately 100 metabolites were quantitated by using CE-TOFMS and enzymatic procedures as described in Materials and Methods. Both PQ- and H_2O_2-mediated oxidative stress resulted in a drastic modulation of several metabolites involved in glycolysis and its associated pathways, and amino acid, nucleotide, and phospholipid metabolism. The changes in the relative levels of quantified metabolites upon oxidative stress as visualized by hierarchical clustering are shown in Fig. 1D. Time course data for metabolites or pathways of

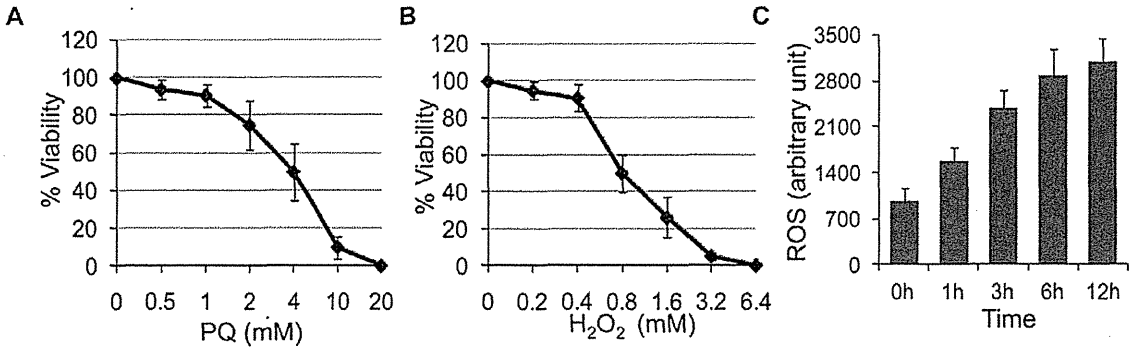

Control = without paraquat (PQ) or H_2O_2
PQ = 1 mM of PQ for 1, 3, 6, or 12 h
H_2O_2 = 0.4 mM of H_2O_2 for 1, 3, 6, or 12 h

Figure 1. PQ- or H_2O_2-mediated oxidative stress causes global metabolic changes. (**A–B**) Survival of *E. histolytica* trophozoites after 12 h of treatment with varying concentrations of PQ (**A**) or H_2O_2 (**B**). The average viability (%) ± standard deviation (SD, error bars) at various concentrations of PQ or H_2O_2 is shown. (**C**) Effect of 1 mM of PQ treatment for 1, 3, 6, or 12 h on the intracellular level of reactive oxygen species. Average level of 2′, 7′-DCF-DA fluorescence (arbitrary units) ±S.D. (error bars) in 5×10^5 cells is shown (**D**) Heat map produced by hierarchical clustering of metabolite profiles obtained from CE-TOFMS analysis. Rows correspond to metabolites and columns correspond to the duration of treatment. Metabolite levels are expressed as fold change with respect to time 0 h. Shades in red and green indicate increase or decrease in the levels of metabolites, respectively, according to the scale bar shown at the bottom.
doi:10.1371/journal.pntd.0001831.g001

particular interest are shown in Fig. 2–4. Metabolomic response to both PQ and H_2O_2 showed similarity in terms of metabolites changed; however, time kinetics of changes in the modulated metabolites is clearly different (Fig. 1D). In addition, PQ- and H_2O_2-specific responses were also detected. In general, when compared to PQ treatment, H_2O_2 treatment caused rapid but mild changes in the metabolome. These differences in the kinetics and magnitude of metabolomic data are likely attributable to nature of these oxidants. H_2O_2 is an oxidizing agent itself, and thus results in faster appearance of the changes in the metabolome, whereas PQ indirectly generates reactive oxygen species resulting in delayed metabolomic response.

Central energy metabolism is repressed by oxidative stress

Like *G. lamblia* and *T. vaginalis*, *E. histolytica* is also microaerophilic, and lacks features of aerobic eukaryotic metabolism, including TCA cycle and oxidative phosphorylation, and generates energy exclusively by substrate level phosphorylation and fermentation [12,39]. Among the metabolites that were measured by CE-TOFMS-based metabolomic analysis, oxidative stress caused modulation of several metabolites involved in central energy metabolism. We observed a general increase in the abundances of the metabolites involved in of the glycolysis and its associated pathways (Fig. 1D and 2). We observed a 2–6-fold

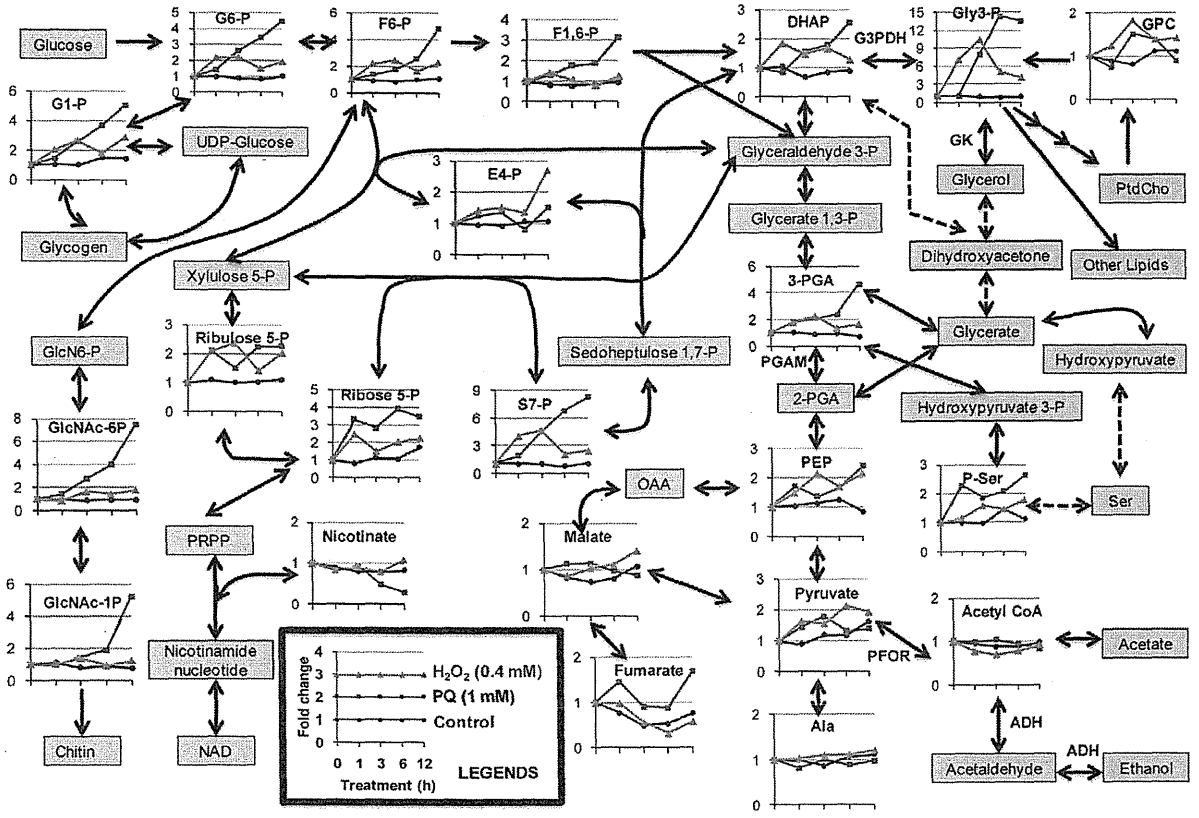

Figure 2. Oxidative stress causes drastic changes in central energy metabolism. The average fold change ± SD (error bars) of metabolites in untreated (control), PQ (1 mM), or H_2O_2 (0.4 mM) treated trophozoites with respect to time 0 h is shown. The enzymes discussed in the text are also shown in bold letters. Abbreviations are: G6-P, glucose 6-phosphate; G1-P, glucose 1-phosphate; F6-P, fructose 6-phosphate; F1,6-P, fructose 1,6-diphosphate; DHAP, dihydroxyacetone phosphate; GPC, glycerophosphocholine; Gly 3-P, glycerol 3-phosphate; 3-PGA, 3-phosphoglycerate; 2-PGA, 2-phosphoglycerate PEP, phosphoenolpyruvate; and P-Ser; O-phosphoserine; E4-P, erythrose 4-phosphate; S7-P, Sedoheptulose 7-phosphate; OAA; oxaloacete; PtdCho, phosphatidylcholine; PFOR, pyruvate:ferredoxin oxidoreductase; PGAM, phosphoglycerate mutase; G3PDH, glycerol 3-phosphate dehydrogenase; GK, glycerol kinase.
doi:10.1371/journal.pntd.0001831.g002

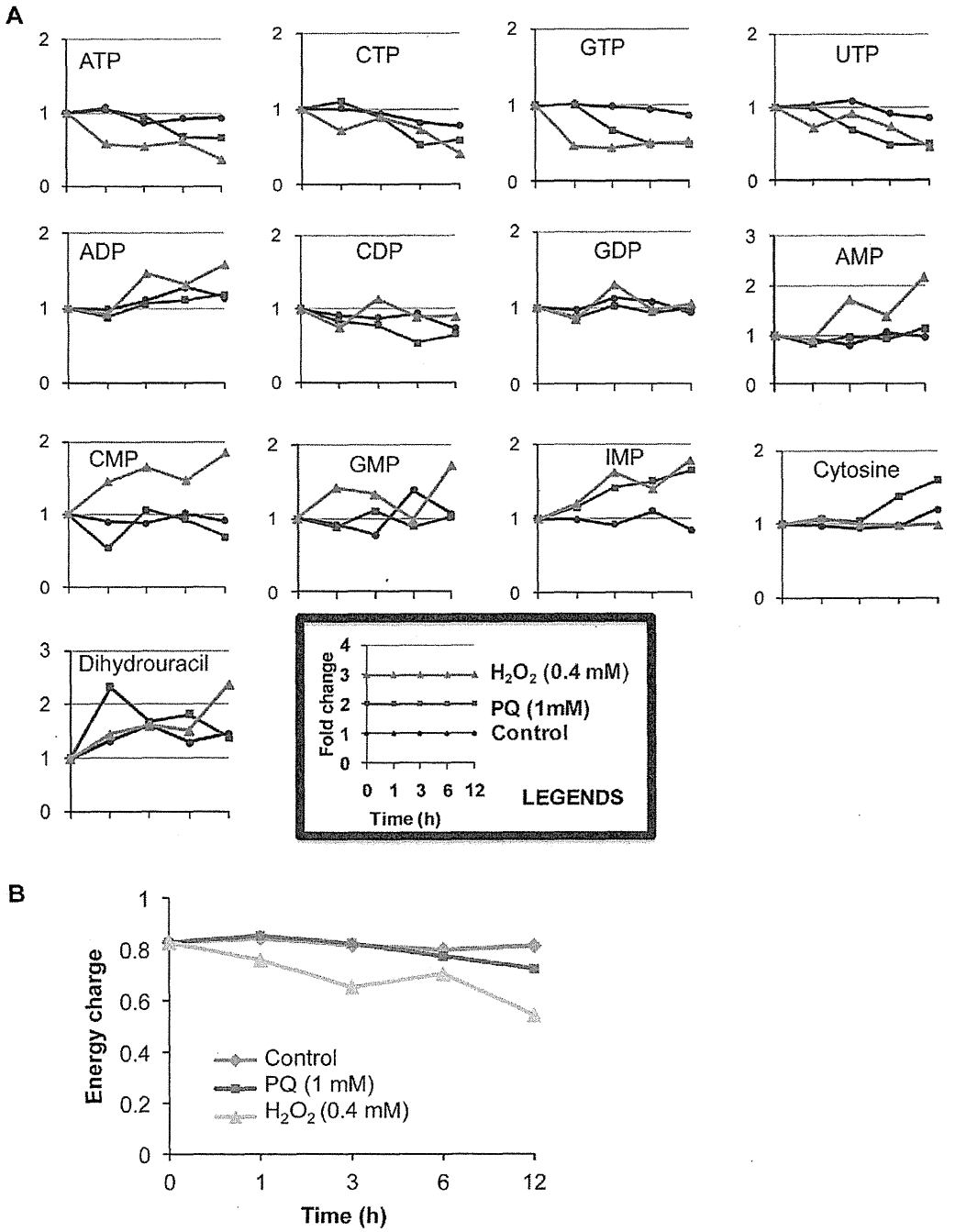

Figure 3. Oxidative stress causes energy depletion. (**A**) The average fold change ± SD (error bars) of the nucleotides at various time points during PQ- or H_2O_2-mediated oxidative stress. (**B**) Adenylate energy charge of the cell, which is calculated by the equation, [(ATP)+1/2(ADP)]/[(ATP)+(ADP)+(AMP)] during the course of oxidative stress.
doi:10.1371/journal.pntd.0001831.g003

increase in most of the glycolytic intermediates from glucose 6-phosphate (G 6-P) to pyruvate, i.e. fructose 6-phosphate (F 6-P), fructose 1, 6-diphosphate (F 1,6-P), dihydroxyacetone phosphate (DHAP), 3-phosphoglycric acid (3-PGA), and phosphoenolpyruvate, upon oxidative stress caused by both PQ and H_2O_2. We also expected a similar increment in the level of glyceraldehyde 3-phosphate. However, due to its high turnover or low stability, the metabolite was undetected using CE-TOFMS. The accumulation of these glycolytic intermediates suggests that there is a relative decrease in the flux through pathways downstream of glycolysis. In contrast to the significant increase in the abundance of glycolytic intermediates upstream of pyruvate upon oxidative stress, we

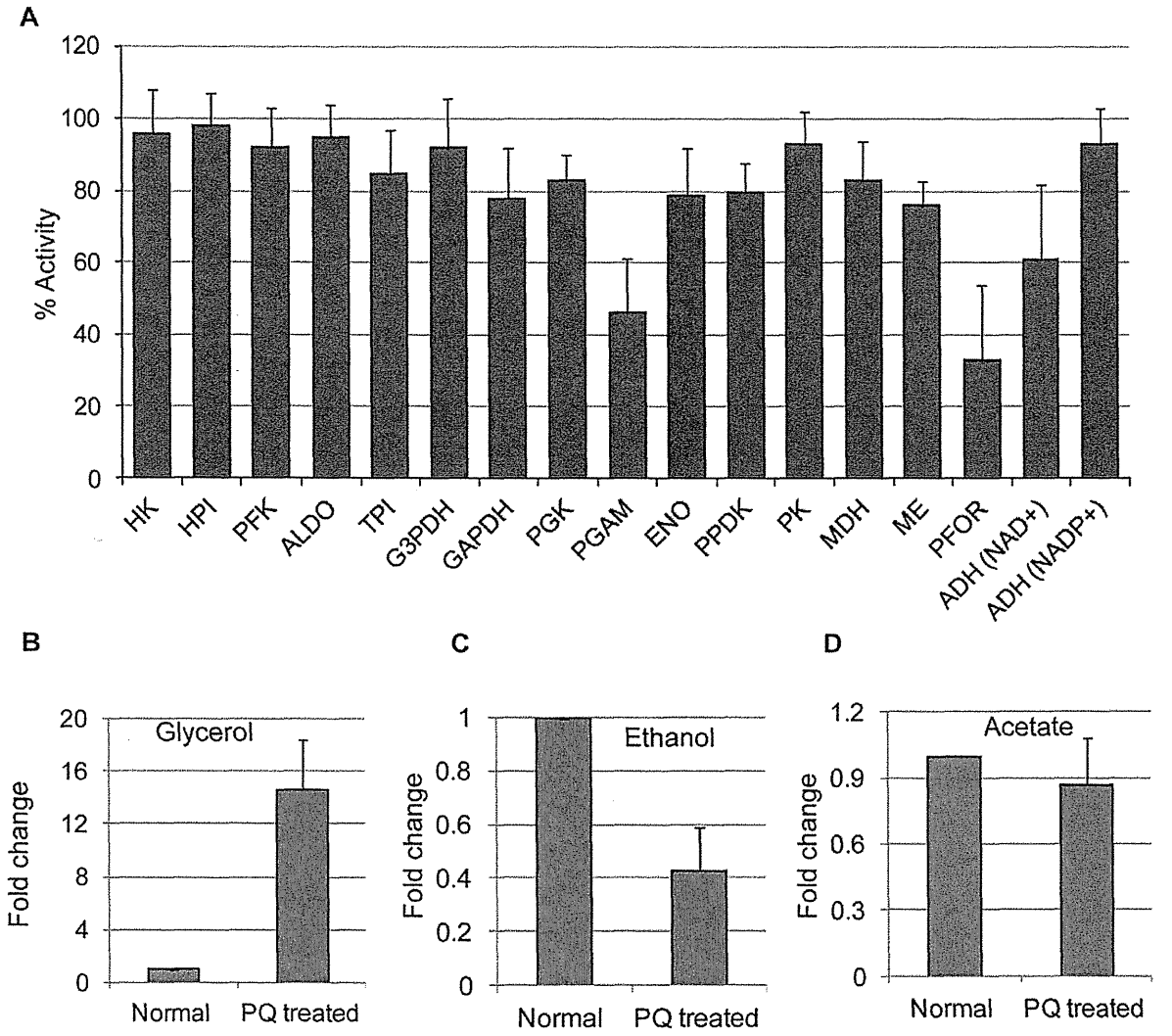

Figure 4. Oxidative stress inactivates glycolytic enzymes and redirects glycolytic flux towards glycerol synthesis. (**A**) Activities of enzymes involved in the central energy metabolism upon PQ (1 mM for 12 h) treatment. Enzymatic activities are expressed as percentage relative to untreated trophozoites. (**B–D**) The average fold change ± SD (error bars) of glycerol, ethanol, and acetate in untreated (control) or PQ-treated (1 mM for 12 h) trophozoites are shown. Abbreviations are: HK, Hexokinase; HPI, Hexose phosphate isomerase; PFK, Phosphofructokinase; ALDO, Aldolase; TPI, Triose-phosphate isomerase; GAPDH, glyceraldehyde 3-P dehydrogenase; PGK, Phosphoglycerate kinase; ENO, Enolase; PPDK, Pyruvate phosphate dikinase; PK, Pyruvate kinase; MDH, Malate dehydrogenase; ME, malic enzyme; ADH, Alcohol dehydrogenase.
doi:10.1371/journal.pntd.0001831.g004

observed an approximately 2-fold decrease in ethanol, the major end product of glucose catabolism in *E. histolytica* (Fig. 4C, see below), supporting the premise that the glycolytic flux downstream of pyruvate was indeed repressed. However, no significant change in acetate production was observed (Fig. 4D, see below). In addition, we also found that upon oxidative stress the accumulated glycolytic metabolites were re-routed towards pathways associated with glycolysis. For example, the metabolites are re-directed towards chitin biosynthetic pathway, glycerol production via glycerol 3-phosphate, and O-phosphoserine, an immediate precursor of L-serine. Accumulation of glycolytic intermediates hints repression of glycolysis as result of free radical-mediated inactivation of key glycolytic enzymes. Accumulation of glycolytic intermediates such as pyruvate, glucose 6-phosphate and fructose 6-phosphate, and repression of glycolytic flux upon oxidative or nitrosative stress has previously been shown in *E. histolytica* [40,41]. Ramos-Martínez, E. *et al.* [40] reported accumulation of G 6-P, F 6-P, and DHAP, and decrement in ATP and ethanol production upon SNP (sodium nitroprusside, nitric oxide producer) mediated apoptosis in *E. histolytica*. Similarly, an acumulation of G 6-P, F 6-P, and pyruvate, and decrement in ATP and ethanol was also reported in *E. histolytica* exposed to hyperbaric oxygen [41]. Although the nature of changes in selected glycolytic intermediates and ATP upon oxidative or nitrosative stress reported in the previous studies was similar to that in the present study, the magnitude of these changes varies. For example, Ramos-Martínez E. *et al.* [41] reported a 6–7 fold increment in the level of pyruvate, whereas niether PQ nor H_2O_2 treatment caused >2 fold change in our study. These differences are likely due to chemical nature, concentrations and the exposure time of oxidants, experimental

design, and the methods of metabolite quantitation. We should also emphasize that our CE-TOFMS-based method to quantitate charged metabolites is far more sensitive than the enzyme-based quantitation methods used previously.

Non-oxidative pentose phosphate pathway is replenished by oxidative stress

The pentose phosphate pathway (PPP) is, in general, an anabolic pathway that generates ribose-5-phosphate for the synthesis of the nucleotides and nucleic acids, and reducing equivalents, in the form of NADPH, for reductive biosynthetic processes. PPP is widely distributed, and found in most prokaryotes and eukaryotes. However, PPP is not functional in *E. histolytica*, which lacks glucose 6-phosphate dehydrogenase (G6PDH) and transaldolases [12]. As shown in Fig. 1D and 2, most intermediates of the non-oxidative branch of PPP were increased upon oxidative stress. Erythrose 4-phosphate (E4-P), ribulose 5-phosphate (ribulose 5-P), and ribose 5-phosphate (ribose 5-P) showed 1.5 to 4-fold increments. Moreover, sedoheptulose 7-phosphate (S7-P) showed a maximum increment of 5 to 9 fold upon PQ or H_2O_2 treatment. Changes in all of these metabolites appear earlier upon H_2O_2 treatment, compared to PQ-mediated oxidative stress.

As described above, most of the intermediates of glycolysis upstream of acetylCoA were accumulated upon oxidative stress. These data indicate that oxidative stress blocks glycolysis, while glucose uptake continues, leading to accumulation and redirection of the metabolic flux from glycolysis to associated pathways. *E. histolytica* lacks G6PDH and transaldolase; however, it possesses an alternative hexose-pentose interconversion pathway that does not require transaldolases, but depends on three enzymes: phospho-fructokinase, transketolase, and aldolase [42]. Thus, our data validate the previous reports of presence and functionality of such non-oxidative hexose-pentose inter-conversion pathway in *E. histolytica* [42].

It has been shown in yeast that oxidative stress redirects metabolic flux from glycolysis to PPP, leading to generation of NADPH [8]. However, such a redirection of metabolic flux in *E. histolytica* does not generate NADPH as it lacks the oxidative branch of PPP; however, this redirection results in the accumulation of several intermediates of non-oxidative branch of PPP using the alternative hexose-pentose interconversion pathway [42]. These data indicate an additional NADPH-independent role of the non-oxidative branch of PPP. A recent report has indeed shown such an NADPH-independent role of non-oxidative PPP intermediates in transcriptional re-programming after oxidative stress [43]. It was shown that the blockade of or the increment in the production of sedoheptulose 7-phosphate and other intermediates of the non-oxidative branch of PPP decreased or increased tolerance against oxidants, respectively [43]. Although a protective role of these intermediates was previously discussed in yeast [43], it needs to be further tested whether it is also a case for *E. histolytica* because it lacks oxidative branch of the pentose phosphate pathway. In addition, ribose 5-phosphate synthesized in this pathway is also a precursor of NAD, which is used by NAD kinase to synthesize NADP ([44], and Jeelani et al. unpublished). NADP is further used by pyridine nucleotide trans-hydrogenase to synthesize NADPH using electrochemical proton gradient [17].

Activation of chitin biosynthetic pathway

E. histolytica exists in two morphologically distinct forms during its life cycle: the proliferative, non-infective, but pathogenic trophozoite form, and the dormant non-pathogenic, but infective, cyst form. The surface of the cysts is protected with the cell wall composed of chitin [45,46]. We observed activation of the chitin biosynthetic pathway upon oxidative stress. Two key intermediates of this pathway, namely N-acetylglucosamine 6-phosphate (GlcNAc 6-P) and N-acetylglucosamine 1-phosphate (GlcNAc 1-P) were increased upon oxidative stress. However, PQ-mediated oxidative stress caused more dramatic increments (5–8-fold), compared to H_2O_2 (1.5–2.0-fold). These results suggest that oxidative stress may serve as an environmental stimulus to trigger encystation. Indeed, H_2O_2 at the concentration 10-fold higher than that used in this study (4 vs. 0.4 mM) was shown to induce glucosamine 6-phosphate isomerase, an enzyme that interconverts GlcNAc 6-P and GlcNAc 1-P, and formation of cyst-like structures in *E. histolytica* [47]. In addition, oxidative stress has also been shown to induce differentiation of *G. lamblia* [48]. One of the possible reasons of the induction of the chitin biosynthetic pathway may be that trophozoite needs to transform into the dormant cyst form, which is tolerant to the adverse external environments. In addition, it was also suggested that chitin oligosaccharides can also serve as potent antioxidants by scavenging free radicals [49].

Oxidative stress modulates nucleotide metabolism

As glycolysis is the major source of energy generation in *E. histolytica*, a reduced glycolytic flux is expected to cause depletion of the energy content in the trophozoites. As expected, the levels of the nucleoside triphosphates, ATP, GTP, UTP, and CTP, were significantly decreased upon oxidative stress (Fig. 3A). In contrast, the levels of nucleoside monophosphates (AMP, CMP, GMP, and IMP) were increased upon H_2O_2 stress, in a manner opposite to the decrement in their corresponding triphosphates counterparts. The levels of nucleoside monophosphates upon PQ-mediated oxidative stress remain unchanged except IMP, which was increased in a time-dependent manner. We also examined the average adenylate energy charge during oxidative stress (Fig. 3B). Energy charge was decreased upon oxidative stress; however, the decrement was more prominent by H_2O_2 stress compared to PQ-mediated oxidative stress. The decrement in nucleoside triphosphates and energy charge is consistent with the repression of glycolysis, which is also evident by the accumulation of glycolytic intermediates, and decreased ethanol production (Fig. 2 and 4C). We also quantitated the levels of nicotinamide nucleotides in trophozoites exposed to PQ-mediated oxidative stress (data not shown). The level of NAD was decreased, whereas the level of NADP was increased upon paraquat treatment for 12 h. However, the levels of reduced form of these nicotinamide nucleotides only slightly decreased (data not shown).

Modulation of sulfur-containing amino acid metabolism

Amino acid metabolism in *E. histolytica* is important in generating ATP by amino acid catabolism [50]. In addition, *E. histolytica* possesses unique pathways for the synthesis and degradation of sulfur-containing amino acids and their derivatives. For example, it lacks functional trans-sulfuration pathways, but possesses methionine γ-lyase for the degradation of sulfur-containing amino acids [51–54]. Furthermore, it also possesses unique *de novo* methanethiol or sulfur (sulfide) assimilatory pathways for the synthesis of S-methylcysteine or L-cysteine, respectively [30,51,52]. As amino acid metabolism plays an important role in the biology of *E. histolytica*, we also examined the effects of oxidative stress on the amino acid level. Both PQ and H_2O_2-mediated oxidative stress led to decrements in L-cysteine and L-cystine, and slight increment in cysteine S-sulfinate, in a time-dependent manner (Figure S1). These data suggest that in *E. histolytica* L-cysteine is likely involved in the scavenging of oxygen free radicals. The concomitant decrement in L-cystine also highlights the significance of NADPH-dependent oxidoreductase,

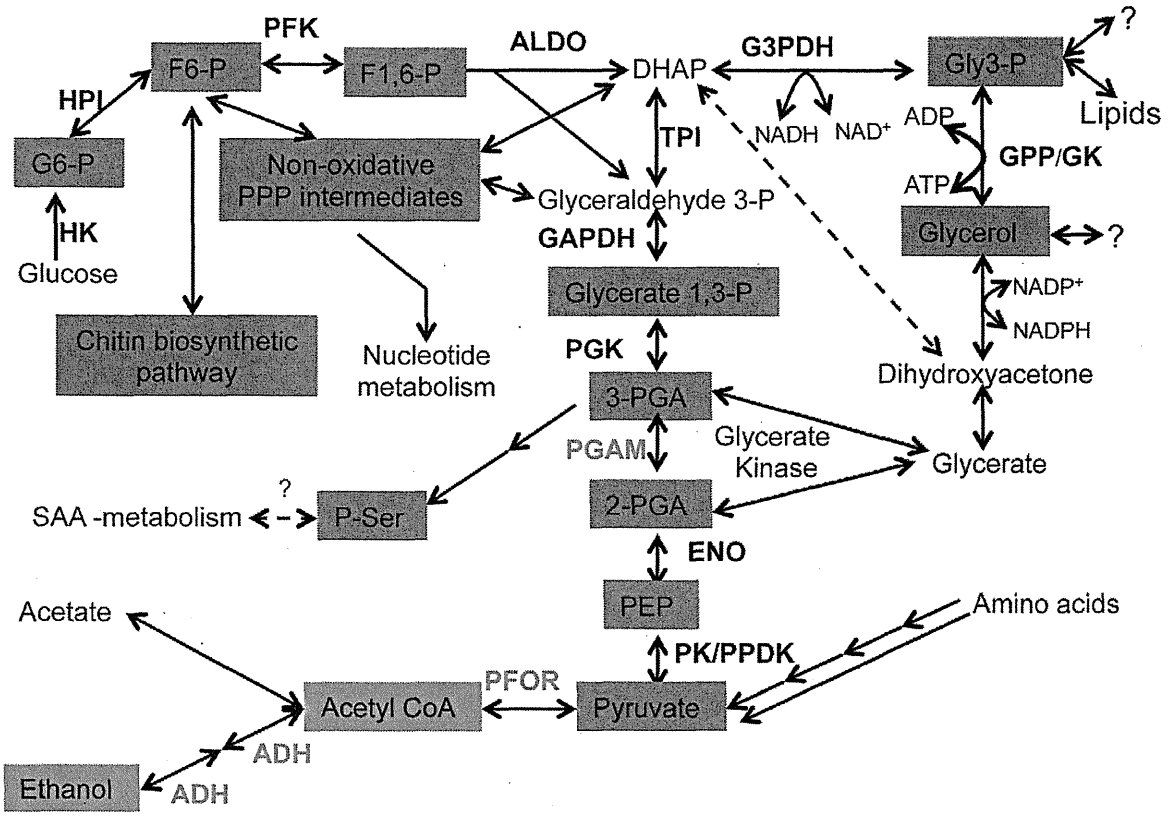

Figure 5. Representation of major changes in central carbon metabolism upon oxidative stress. Shades in red and green indicate increase or decrease of metabolites, respectively. Enzymes catalyzing these reactions are also shown in bold letters. Enzymes in black or green are those whose activities were unchanged or downregulated, respectively, upon oxidative stress. Abbreviations are: HK, Hexokinase; HPI, Hexose phosphate isomerase; PFK, Phosphofructokinase; ALDO, Aldolase; TPI, Triose-phosphate isomerase; GAPDH, glyceraldehyde 3-P dehydrogenase; PGK, Phosphoglycerate kinase; ENO, Enolase; PPDK, Pyruvate phosphate dikinase; PK, Pyruvate kinase; MDH, Malate dehydrogenase; ME, malic enzyme; ADH, Alcohol dehydrogenase; GK, glycerol kinase; GPP, glycerol 3-phosphate phosphatase.
doi:10.1371/journal.pntd.0001831.g005

which functions as cystine reductase to replenish L-cysteine [55]. We also observed a time-dependent increment in S-methylcysteine, which is synthesized from O-acetylserine and methanethiol [30]. Synthesis of S-methylcysteine upon oxidative stress suggests activation of serine acetyltransferases (SAT1 and SAT2) due to reversal of their inhibition by L-cysteine [56]. As mentioned above, the level of O-phosphoserine, a precursor of L-serine and L-cysteine [51,52], was significantly increased in a time-dependent manner upon oxidative stress, whereas that of L-serine remained unchanged. Since O-phosphoserine phosphatase, an enzyme that converts O-phosphoserine to L-serine, has not been identified in *E. histolytica*, serine biosynthesis may not occur under the conditions used in the study. Thus, the fate of O-phosphoserine in *E. histolytica* still remains to be established. Apart from these limited changes, we did not observed any significant change in other amino acids.

Oxidative stress inactivates key metabolic enzymes

Glycolytic enzymes are known to be highly susceptible to inhibition by reactive oxygen species [57,58]. We assayed activities of several key enzymes of glycolysis and its associated pathways upon PQ-mediated oxidative stress. Among the tested enzymes, the activities of PFOR, phosphoglycerate mutase (PGAM), and NAD^+ dependent alcohol dehydrogenase (ADH) were decreased to 33±21, 46±15, and 61±21%, respectively. However, the activities of GAPDH, TPI, PGK, ENO, and PPDK were decreased by only 16–22%, and the activities of remaining enzymes were not significantly changed (Fig. 4A). PFOR and ADH have previously been shown to be inactivated by O_2-mediated oxidative stress in *E. histolytica* [22]. In addition to PFOR, we also found that PGAM was inactivated by PQ-mediated superoxide stress. However, PGAM was not found to be inhibited by O_2-mediated oxidative stress [20]. Thus inhibition of PGAM may be specific to PQ generated superoxide radicals. As PGAM is a glycolytic flux-regulating enzyme in *E. histolytica* [59], its inactivation will have more effect on glycolytic activity, and hence cause the redirection of flux towards associated pathways. Thus, drastic inhibition of PGAM, PFOR and ADH, and partial inhibition of other glycolytic enzymes resulted in the overall reduction in glycolytic flux, and accumulation of glycolytic intermediates.

Redirection of metabolic flux towards glycerol production upon oxidative stress

Identification of glycerol 3-phosphate dehydrogenase (G3PDH) and glycerol kinase (GK) in the genome of *E. histolytica* suggests the presence of glycerol metabolism in this parasite [12]. However, the activity of G3PDH in the soluble fraction of *E. histolytica* was not detected by conventional enzymatic methods [60], and it was

proposed that dihydroxyacetone phosphate (DHAP) is mainly used for triglyceride synthesis, but not glycerol 3-phosphate (G 3-P). In contrast, as shown in Fig. 2, we found Gly 3-P as one of the most highly modulated (10–14 fold) metabolites upon oxidative stress. The drastic accumulation of Gly 3-P, together with the increase in other upstream glycolytic intermediates, upon oxidative stress clearly suggests the presence of functional G3PDH in this parasite. We also tested if accumulated Gly 3-P is also converted to glycerol leading to its accumulation. As shown in Fig. 4B, the level of intracellular glycerol was also dramatically increased upon PQ-mediated oxidative stress. As the changes in the levels of Gly 3-P and glycerol were similar in terms of fold changes, most of Gly 3-P produced upon oxidative stress is likely converted to glycerol. We also assayed production of ethanol and acetate upon PQ-mediated oxidative stress, and found that ethanol production was significantly decreased, while the acetate level remained unchanged (Fig. 4, C and D). These data indicate that *E. histolytica* is capable of glycerol biosynthesis from glucose, similar to other protozoa such as *T. vaginalis*, *Trypanosoma brucei*, and *Plasmodium falciparam* [61–63].

While importance of glycerol metabolism in oxidative stress defense has previously been shown [64], its specific induction upon oxidative stress was not reported. In yeast, it was shown that Gly 3-P was converted to glycerol by the action of Gly 3-P phosphatase (GPP), and deletion of this gene resulted in the increased sensitivity of yeast to peroxide and superoxide stress [64]. Although glycerol functions as an efficient free radical scavenger, other mechanisms by which glycerol protects against oxidative stress are equally possible. One of these alternative mechanisms is the NADP-dependent conversion of glycerol to dihydroxyacetone (by glycerol dehydrogenase) or glyceraldehyde (by glyceraldehyde reductase), leading to the formation of NADPH (Fig. 5). DHAP generated in this reaction may then be converted to dihydroxyacetone phosphate. Glyceraldehyde can be converted to glycerate, and subsequently enter glycolysis as 2-phosphoglycerate bypassing PGAM, which is one of the flux-controlling enzymes targeted by free radicals (Fig. 4A, and Fig. 5). We also showed that increment in Gly 3-P also led to equivalent increment in glycerol. Two enzymes, GPP and GK, may catalyze the conversion of Gly 3-P to glycerol (Fig. 5). As *E. histolytica* lacks GPP, GK is likely responsible for the conversion, which generates ATP (Fig. 5). Thus, an alternative role of redirection of metabolic flux towards glycerol may be to generate energy from accumulated glycolytic intermediates. Conversion of one molecule of DHAP to ethanol or acetate generates 2 or 3 ATP molecules, respectively. In contrast, synthesis of glycerol from DHAP by the sequential action of G3PDH and GK generates only one ATP molecule. Thus, redirection of glycolytic flux towards glycerol reduces efficiency of energy generation, but may still be beneficial for the trophozoites to extract the energy contained in the accumulated glycolytic intermediates upon oxidative stress. Further studies are needed to precisely determine the role of glycerol metabolism in generation of ATP and reducing powers under oxidative stress in *E. histolytica*.

Conclusions

In the present study, we demonstrated that exposure to oxidative stress led to drastic metabolic changes in *E. histolytica*. While the expression of genes involved in the metabolism was only slightly affected by oxidative stress, several key enzymes involved in glycolysis were inactivated to re-direct the metabolic flux towards the associated pathways such as the non-oxidative branch of PPP, chitin, and glycerol biosynthetic pathways (Fig. 5). We also demonstrated the functionality of G3PDH, and showed, like other protozoan parasites, that GK in *E. histolytica* is capable of catalyzing the reverse reaction, leading to formation of glycerol and ATP (Fig. 5). Detailed biochemical and functional analysis of G3PDH and GK is necessary to understand the role of glycerol metabolism in the energy metabolism and oxidative stress tolerance. It is also important to know the fate and physiological significance of increased production of glycerol 3-phosphate and glycerol upon oxidative stress.

Supporting Information

Figure S1 Oxidative stress modulates amino acid metabolism. The average fold change ± SD (error bars) of metabolites in untreated (control), H_2O_2, or PQ treated trophozoites with respect to time 0 h is shown. Abbreviations are: SAM, S-adenosylmethionine; SAH, S-adenosylhomocysteine; dcSAMd, decarboxylated S-adenosylmethionine; 5-MTA, 5′-methylthioadenosine; PEP, Phosphoenolpyruvate; MetSO, Methionine sulfoxide; OAS, O-acetylserine; SMC, S-methylcysteine; P-Ser, O-phosphoserine; 3-PGA, 3-phosphoglycerate.
(TIF)

Acknowledgments

We thank Kumiko Nakada-Tsukui, Masahiro Sugimoto, and Akiyoshi Hirayama and all members of our laboratory for technical assistance and valuable discussions.

Author Contributions

Conceived and designed the experiments: AH DS GJ TN. Performed the experiments: AH DS GJ. Analyzed the data: AH DS GJ. Contributed reagents/materials/analysis tools: TS TN. Wrote the paper: AH TN.

References

1. Imlay JA (2003) Pathways of oxidative damage. Annu Rev Microbiol 57: 395–418.
2. Apel K, Hirt H (2004) Reactive oxygen species: metabolism, oxidative stress, and signal transduction. Annu Rev Plant Biol 55: 373–399.
3. Perrone GG, Tan SX, Dawes IW (2008) Reactive oxygen species and yeast apoptosis. Biochim Biophys Acta 1783: 1354–1368.
4. Clement MV, Pervaiz S (1999) Reactive oxygen intermediates regulate cellular response to apoptotic stimuli: an hypothesis. Free Radic Res 30: 247–252.
5. Nandi N, Sen A, Banerjee R, Kumar S, Kumar V, Ghosh AN, Das P (2010) Hydrogen peroxide induces apoptosis-like death in *Entamoeba histolytica* trophozoites. Microbiol 156: 1926–41.
6. Ghosh AS, Dutta S, Raha S (2010) Hydrogen peroxide-induced apoptosis-like cell death in *Entamoeba histolytica*. Parasitol Int 59:166–72.
7. Temple MD, Perrone GG, Dawes IW (2005) Complex cellular responses to reactive oxygen species. Trends Cell Biol 15: 319–326.
8. Ralser M, Walmelink MM, Kowald A, Gerisch B, Heeren G, et al. (2003) Dynamic re-routing of the carbohydrate flux is key to counteracting oxidative stress. J Biol 6: 10.
9. Stanley SL, Jr (2003) Amoebiasis. Lancet 361: 1025–1034.
10. Weinbach, E. C., and Diamond L. S. (1974) *Entamoeba histolytica*. I. Aerobic metabolism. Exp. Parasitol 35: 232–243.
11. Bogdan C, Rollinghoff M, Diefenbach A (2000) Reactive oxygen and reactive nitrogen intermediates in innate and specific immunity. Curr Opin Immunol 12: 64–76.
12. Loftus B, Anderson I, Davies R, Alsmark UC, Samuelson J, et al. (2005) The genome of the protist parasite *Entamoeba histolytica*. Nature 433: 865–868.
13. Mehlotra RK (1996) Antioxidant defense mechanisms in parasitic protozoa. Crit Rev Microbiol 22: 295–314.
14. Fahey RC, Newton GL, Arrick B, Overdank-Bogart T, Aley SB (1984) *Entamoeba histolytica*: a eukaryote without glutathione metabolism. Science 224: 70–72.
15. Saraiva LM, Vicente JB, Teixeira M (2004) The role of the flavodiiron proteins in microbial nitric oxide detoxification. Adv Microb Physiol 49: 77–129.
16. Sen A, Chatterjee NS, Akbar MA, Nandi N, et al. (2007) The 29-kilodalton thiol-dependent peroxidase of *Entamoeba histolytica* is a factor involved in pathogenesis and survival of the parasite during oxidative stress. Eukaryot Cell 6: 664–673.

17. Jackson JB (1991) The proton-translocating nicotinamide adenine dinucleotide transhydrogenase. J Bioenerg Biomembr 23: 715–741.
18. Yousuf MA, Mi-ichi F, Nakada-Tsukui K, Nozaki T (2010) Localization and targeting of an unusual pyridine nucleotide transhydrogenase in *Entamoeba histolytica*. Eukaryot Cell 9: 926–33.
19. Vicente J, Ehrenkaufer G, Saraiva L, Teixeira M, Singh U (2008) *Entamoeba histolytica* modulates a complex repertoire of novel genes in response to oxidative and nitrosative stresses: implications for amebic pathogenesis. Cell Microbiol 11: 51–69.
20. Godon C, Lagniel G, Lee J, Buhler JM, Kieffer S, et al. (1998)The H2O2 stimulon in *Saccharomyces cerevisiae*. J Biol Chem 273: 22480–224892.
21. Demple B, Amabile-Cuevas CF (1991) Redox redux: the control of oxidative stress responses. Cell 67: 837–839.
22. Pineda E, Encalada R, Rodríguez-Zavala JS, Olivos-García A, Moreno-Sánchez R, Saavedra E (2010) Pyruvate:ferredoxin oxidoreductase and bifunctional aldehyde-alcohol dehydrogenase are essential for energy metabolism under oxidative stress in *Entamoeba histolytica*. FEBS J 277: 3382–3395.
23. Morrison HG, McArthur AG, Gillin FD, Aley SB, Adam RD, Olsen GJ, et al. (2007) Genomic minimalism in the early diverging intestinal parasite *Giardia lamblia*. Science 317: 1921–1926.
24. Carlton JM, Hirt RP, Silva JC, Delcher AL, Schatz M, Zhao Q, et al. (2007) Draft genome sequence of the sexually transmitted pathogen Trichomonas vaginalis. Science 315: 207–212.
25. Soga T, Baran R, Suematsu M, Ueno Y, Ikeda S, et al. (2006) Differential metabolomics reveals ophthalmic acid as an oxidative stress biomarker indicating hepatic glutathione consumption. J Biol Chem 281: 16768–16776.
26. Sato S, Soga T, Nishioka T, Tomita M (2004) Simultaneous determination of the main metabolites in rice leaves using capillary electrophoresis mass spectrometry and capillary electrophoresis diode array detection. Plant J 40: 151–163
27. Soga T, Ohashi Y, Ueno Y, Naraoka H, Tomita M, Nishioka T (2003) Quantitative metabolome analysis using capillary electrophoresis mass spectrometry. J Proteome Res 2: 488–494.
28. Diamond LS, Harlow DR, Cunnick CC (1978) A new medium for the axenic cultivation of *Entamoeba histolytica* and other *Entamoeba*. Trans R Soc Trop Med Hyg 72: 431–432.
29. Clark CG, Diamond LS (2002) Methods for cultivation of luminal parasitic protists of clinical importance. Clin Microbiol Rev 15: 329–341.
30. Husain A, Sato D, Jeelani G, Mi-ichi F, Ali V, Suematsu M, Soga T, Nozaki T (2010) Metabolome analysis revealed increase in S-methylcysteine and phosphatidylisopropanolamine synthesis upon L-cysteine deprivation in the anaerobic protozoan parasite *Entamoeba histolytica*. J Biol Chem 285: 39160–39170.
31. Jeelani G, Sato D, Husain A, Escueta-de Cadiz A, Sugimoto M, et al. (2012) Metabolic profiling of the protozoan parasite *Entamoeba invadens* revealed activation of unpredicted pathway during encystation. PLoS ONE 7(5): e37740.
32. Ohashi Y, Hirayama A, Ishikawa T, Nakamura S, Shimizu K, et al. (2008) Depiction of metabolome changes in histidine-starved *Escherichia coli* by CE-TOFMS. Mol Biosyst 4: 135–147.
33. Soga T, Heiger DN (2000) Amino acid analysis by capillary electrophoresis electrospray ionization mass spectrometry. Anal Chem 72:1236–1241.
34. Soga T, Ueno Y, Naraoka H, Ohashi Y, Tomita M, Nishioka T (2002) Simultaneous determination of anionic intermediates for Bacillus subtilis metabolic pathways by capillary electrophoresis electrospray ionization mass spectrometry. Anal Chem 74: 2233–2239.
35. Soga T, Igarashi K, Ito C, Mizobuchi K, Zimmermann HP, Tomita M (2009) Metabolomic profiling of anionic metabolites by CE-MS. Anal Chem 81: 6165–6174.
36. Sugimoto M, Wong DT, Hirayama A, Soga T, Tomita M (2010) Capillary electrophoresis mass spectrometry-based saliva metabolomics identified oral, breast and pancreatic cancer-specific profiles. Metabolomics 6: 78–95.
37. Smith CA, Want EJ, O'Maille G, Abagyan R, Siuzdak G (2006) XCMS: processing mass spectrometry data for metabolite profiling using nonlinear peak alignment, matching, and identification. Anal Chem 78: 779–87.
38. Baran R, Kochi H, Saito N, Suematsu M, Soga T, Nishioka T, et al. (2006) MathDAMP: a package for differential analysis of metabolite profiles. BMC Bioinformatics 13: 530.
39. Clark CG, Alsmark UC, Tazreiter M, Saito-Nakano Y, Ali V, Marion S (2007) Structure and content of the *Entamoeba histolytica* genome. Adv Parasitol 65: 51–190.
40. Ramos-Martínez E, Olivos-García A, Saavedra E, Nequiz M, Sánchez EC, et al. (2009) *Entamoeba histolytica*: oxygen resistance and virulence. Int J Parasitol 39: 693–702.
41. Ramos -Martínez E, Olivos-García A, Nequiz M, Saavedra E, Tello E, et al. (2007) *Entamoeba histolytica*: apoptosis induced in vitro by nitric oxide species. Exp Parasitol 116: 257–65.
42. Susskind BM, Warren LG, Reeves RE (1982) A pathway for the interconversion of hexose and pentose in the parasitic amoeba *Entamoeba histolytica*. Biochem J 204: 191–196.
43. Krüger A, Grüning NM, Wamelink MM, Kerick M, Kirpy A, et al. (2011) The pentose phosphate pathway is a metabolic redox sensor and regulates transcription during the antioxidant response. Antioxid Redox Signal 15(2): 311–24.
44. Pollak N, Dolle C, Ziegler M (2007) The power to reduce: pyridine nucleotides-small molecules with a multitude of functions. Biochem J 402:205–218
45. Arroyo-Begovich A, Carabez-Trejo A, Ruíz-Herrera J (1978) Composition of the cell wall of Entamoeba invadens cysts. Arch Invest Med (Mex) 9: 99–104.
46. Chávez-Munguía B, Martínez-Palomo A (2011) High-resolution electron microscopical study of cyst walls of *Entamoeba spp*. J Eukaryot Microbiol 58: 480–486.
47. Aguilar-Diaz H, Diaz-Gallardo M, Laclette JP, Carrero JC (2010) *In vitro* Induction of *Entamoeba histolytica* Cyst-like Structures from Trophozoites. PLoS Negl Trop Dis 4(2) :e607.
48. Luján HD, Mowatt MR, Nash TE (1997) Mechanisms of *Giardia lamblia* differentiation into cysts. Microbiol Mol Biol Rev 61 :294–304.
49. Ngo DN, Kim MM, Kim SK (2008) Chitin oligosaccharides inhibit oxidative stress in live cells. Carbohydr Polym 74: 228–234.
50. Anderson IJ, Loftus BJ (2005) *Entamoeba histolytica*: Observations on metabolism based on the genome sequence. Experimental Parasitology 110: 173–177.
51. Nozaki T, Ali V, Tokoro M (2005). Sulfur-containing amino acid metabolism in parasitic protozoa. Adv Parasitol 60: 1–99.
52. Ali V, Nozaki T (2007) Current therapeutics, their problems, and sulfur-containing amino-acid metabolism as a novel target against infections by "amitochondriate" protozoan parasites. Clin Microbiol Rev 20: 164–187.
53. Tokoro M, Asai T, Kobayashi S, Takeuchi T, Nozaki T (2003) Identification and characterization of two isoenzymes of methionine gamma-lyase from *Entamoeba histolytica*: a key enzyme of sulfur-amino acid degradation in an anaerobic parasitic protest that lacks forward and reverse trans-sulfuration pathways. J Biol Chem 278: 42717–42727.
54. Husain A, Jeelani G, Sato D, Nozaki T (2011) Global analysis of gene expression in response to L-Cysteine deprivation in the anaerobic protozoan parasite *Entamoeba histolytica*. BMC Genomics 12: 275.
55. Jeelani G, Husain A, Sato D, Ali V, Suematsu M, Soga T, Nozaki T (2010) Two atypical L-cysteine-regulated NADPH-dependent oxidoreductases involved in redox maintenance, L-cystine and iron reduction, and metronidazole activation in the enteric protozoan Entamoeba histolytica. J Biol Chem 285: 26889–26899.
56. Hussain S, Ali V, Jeelani G, Nozaki T (2009) Isoform-dependent feedback regulation of serine O-acetyltransferase isoenzymes involved in L-cysteine biosynthesis of Entamoeba histolytica. Mol Biochem Parasitol 2009 Jan;163(1):39–47.
57. Shenton D, Grant CM (2003) Protein S-thiolation targets glycolysis and protein synthesis in response to oxidative stress in the yeast *Saccharomyces cerevisiae*. Biochem J 374: 513–519.
58. Colussi C, Albertini MC, Coppola S, Rovidati S, Galli F, Ghibelli L (2000) H2O2-induced block of glycolysis as an active ADP-ribosylation reaction protecting cells from apoptosis. FASEB J 14: 2266–2276.
59. Saavedra E, Marín-Hernández A, Encalada R, Olivos A, Mendoza-Hernández G, Moreno-Sánchez R (2007) Kinetic modeling can describe in vivo glycolysis in *Entamoeba histolytica*. FEBS J 274: 4922–4940.
60. Reeves RE, Lobelle-Rich P (1983) Absence of alpha-glycerophosphate dehydrogenase in axenically grown *Entamoeba histolytica*. Am J Trop Med Hyg 32: 1177–1178.
61. Chapman A, Linstead DJ, Lloyd D, Williams J (1985) 13C-NMR reveals glycerol as an unexpected major metabolite of the protozoan parasite *Trichomonas vaginalis*. FEBS 191: 287–92.
62. Hammond DJ, Bowman IB (1980) Studies on glycerol kinase and its role in ATP synthesis in *Trypanosoma brucei*. Mol Biochem Parasitol 2: 77–91.
63. Lian LY, Al-Helal M, Roslaini AM, Fisher N, Bray PG (2009) Glycerol: an unexpected major metabolite of energy metabolism by the human malaria parasite. Malar J 6: 38.
64. Pahlman AK, Granath K, Ansell R, Hohmann S, Adler L (2001)The yeast glycerol 3-phosphatases Gpp1p and Gpp2p are required for glycerol biosynthesis and differentially involved in the cellular responses to osmotic, anaerobic, and oxidative stress. J Biol Chem 276: 3555–3363.

SCIENTIFIC REPORTS

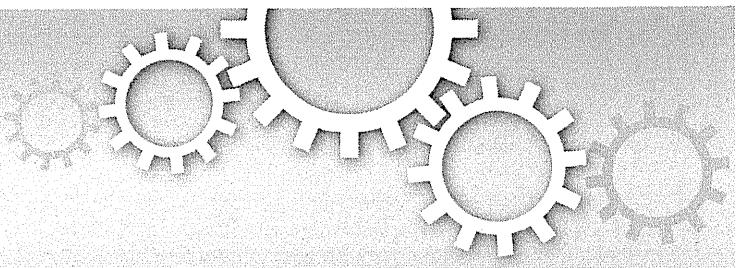

OPEN

SUBJECT AREAS:
EVOLUTION
PARASITOLOGY
MITOCHONDRIA
MOLECULAR EVOLUTION

Received
10 October 2012

Accepted
27 December 2012

Published
24 January 2013

Correspondence and requests for materials should be addressed to T.N. (nozaki@niid.go.jp)

*Current address: Department of Biomolecular Sciences, Faculty of Medicine, Saga University, 5-1-1 Nabeshima, Saga 849-8501, Japan

Novel TPR-containing subunit of TOM complex functions as cytosolic receptor for *Entamoeba* mitosomal transport

Takashi Makiuchi[1,2], Fumika Mi-ichi[1]*, Kumiko Nakada-Tsukui[1] & Tomoyoshi Nozaki[1,3]

[1]Department of Parasitology, National Institute of Infectious Diseases, 1-23-1 Toyama, Shinjuku-ku, Tokyo 162-8640, Japan, [2]Kitasato Institute for Life Sciences and Graduate School of Infection Control Sciences, Kitasato University, Minato-ku, Tokyo 108-8641, Japan, [3]Graduate School of Life and Environmental Sciences, University of Tsukuba, 1-1-1 Tennodai, Tsukuba, Ibaraki 305-8572, Japan.

Under anaerobic environments, the mitochondria have undergone remarkable reduction and transformation into highly reduced structures, referred as *m*itochondrion-*r*elated *o*rganelles (MROs), which include mitosomes and hydrogenosomes. In agreement with the concept of reductive evolution, mitosomes of *Entamoeba histolytica* lack most of the components of the TOM (*t*ranslocase of the *o*uter *m*itochondrial membrane) complex, which is required for the targeting and membrane translocation of preproteins into the canonical aerobic mitochondria. Here we showed, in *E. histolytica* mitosomes, the presence of a 600-kDa TOM complex composed of Tom40, a conserved pore-forming subunit, and Tom60, a novel lineage-specific receptor protein. Tom60, containing multiple tetratricopeptide repeats, is localized to the mitosomal outer membrane and the cytosol, and serves as a receptor of both mitosomal matrix and membrane preproteins. Our data indicate that *Entamoeba* has invented a novel lineage-specific shuttle receptor of the TOM complex as a consequence of adaptation to an anaerobic environment.

Mitochondria are highly divergent structures in eukaryotes, and often reveal degenerate morphology, function, and components in eukaryotes that have been adapted in anoxic or hypoxic environments. Such degenerated mitochondria with reduced or no organellar genome are called mitochondrion-related organelles (MROs), which include mitosomes and hydrogenosomes. While the minimal common function of MROs is still in debate[1–6], protein import of nuclear-encoded proteins into MROs is indispensable for the organisms that possess MROs. All organisms possessing MRO that have been investigated so far, indeed retain at least a gene encoding the core translocation channel Tom40 of the TOM (*T*ranslocase of the *O*uter membrane of *M*itochondria)[7–11]. However, in agreement with the concept of reductive evolution, other components of the canonical aerobic mitochondria such as subunits of TOM, SAM (*S*orting and *A*ssembly *M*achinery), TIM (*T*ranslocase of the *I*nner membrane of *M*itochondria), and small TIM complexes[8,12,13] are often missing in MROs. These data imply two possible scenarios of evolution of mitochondrial protein import: the majority of the import machinery of MROs has been secondarily lost[7,8], or the transport machinery or subunits were replaced with unique and possibly lineage-specific components[14].

The TOM complex is involved in the initial process of the import of nuclear-encoded mitochondrial preproteins into the mitochondria. Remarkable variation exists in the architecture of TOM complexes among eukaryotic lineages. In yeast and mammals, the translocation channel (Tom40), membrane-anchored receptors for the recognition of a targeting signal in preproteins (Tom22, Tom20, and Tom70), and accessory subunits (Tom5, Tom6, and Tom7) consist the TOM complex[15,16]. In plants, an 8-kDa truncated form of Tom22 serves as translocase[17] and chloroplast import receptor Toc64 homolog functions as a TOM component[18], while in trypanosomes, Tom40 appears to be replaced by Omp85 of archaic origin[19]. Tom20, a presequence binding receptor appeared to have independently evolved from two distinct ancestral genes in the animal and plant lineages[20]. Therefore, the investigation of the TOM complex may shed light on the evolution of the protein import machinery of endosymbiont-derived organelles.

Entamoeba histolytica is an anaerobic unicellular parasite, and causes hemorrhagic dysentery and extra intestinal abscesses that are responsible for an estimated 100,000 deaths in endemic areas annually[21]. This parasite possesses mitosomes, and is a good representative of mitochondrial diversification. *Entamoeba* MRO contains the sulfate activation pathway, which has been so far identified only in this organism[9]. Moreover, it lacks a

genome[22], has no membrane potential[22,23], and is devoid of an import system using the canonical transit peptide[9]. Furthermore, *E. histolytica* has none of the homologous subunits of the TOM complex except Tom40[9,13]. This fact, more specifically the lack of Tom20 and Tom70 receptors, suggests that import of mitosomal proteins does not depend on receptor recognition in *Entamoeba*, or that *Entamoeba* possesses an unprecedented receptor subunit undetectable by currently available *in silico* analysis. Here we show that the TOM complex in the *E. histolytica* mitosomes contains a lineage specific subunit, designated Tom60, which is associated with Tom40. Repression of Tom40 or Tom60 by gene silencing shows defects in protein import to mitosomes, and consequently retardation of proliferation. Tom60 is distributed to both the periphery of the mitosomal outer membrane and the cytosol. Moreover, our data strongly suggest that Tom60 is capable to bind *in vitro* to both mitosomal matrix proteins and membrane proteins.

Results

Demonstration of Tom40 localization on *Entamoeba* mitosomes. As we aimed to characterize TOM complex from *Entamoeba*, we first established an *E. histolytica* cell line expressing hemagglutinin (HA)-tagged *E. histolytica* Tom40 (EhTom40) at the carboxyl terminus (Tom40-HA). To verify the expression and mitosomal localization of Tom40-HA, we fractionated lysates from Tom40-HA-expressing trophozoites by two rounds of Percoll gradient ultracentrifugation and analyzed the fractions by immunoblot with anti-HA antibody and anti-Cpn60 antiserum[9]. Cpn60 served as a canonical mitosomal marker. The banding pattern of Tom40-HA among fractions was similar to that of Cpn60 (Supplementary Fig. S1). Next, we carried out the immunofluorescence assay (IFA) using anti-HA antibody and anti-Cpn60 antiserum (Supplementary Fig. S2). Fluorescence signals of Tom40-HA were observed as dotted pattern and were merged with fluorescence signals of Cpn60, suggesting that EhTom40 is localized in mitosomes. Moreover, mitosomal localization of EhTom40 was also supported by immunoelectron microscopy (immuno-EM) (Supplementary Fig. S3) showing that Tom40-HA is concentrated on mitosomal outer membranes.

Identification of 600-kDa *Entamoeba* TOM complex and a novel subunit Tom60. The TOM complex exists in yeast as a ~400-kDa complex, composed of Tom40, Tom22, Tom5, Tom6, and Tom7[24]. To see if *Entamoeba* mitosomes contain TOM complex, and if so, to isolate the whole complex and identify proteins interacting with EhTom40, we investigated an EhTom40-containing complex by blue native polyacrylamide gel electrophoresis (BN-PAGE) followed by immunoblot with anti-HA antibody. Immunoblot analysis of the 100,000 × *g* organelle-enriched fraction of Tom40-HA-expressing trophozoites with anti-HA antibody showed a 600-kDa band (Fig. 1a). To isolate and identify proteins that are associated with the 600-kDa band, the complex was immunoprecipitated with anti-HA antibody (Fig. 1b) and electrophoresed on SDS-PAGE under reducing conditions. A band of approximately 60-kDa in size was detected exclusively in samples co-immunoprecipitated with lysates from the Tom40-HA-expressing trophozoites (Fig. 1c). The band was subjected to liquid chromatography-tandem mass spectrometric analysis (LC-MS/MS), identified to be XP_657124 (Supplementary Fig. S4 and S5, and Supplementary Table S1A), and designated as *E. histolytica* Tom60 (EhTom60). EhTom60 was also detected by LC-MS/MS analysis of the 600-kDa complex (Supplementary Table S1B). The protein was previously identified in our mitosome proteome[9].

Lineage specific distribution of Tom60. Tom60 appears to be uniquely present in the genus. Tom60 orthologs were found in *E. dispar* and *E. invadens* (EDI_218540 and EIN_149090, respectively)

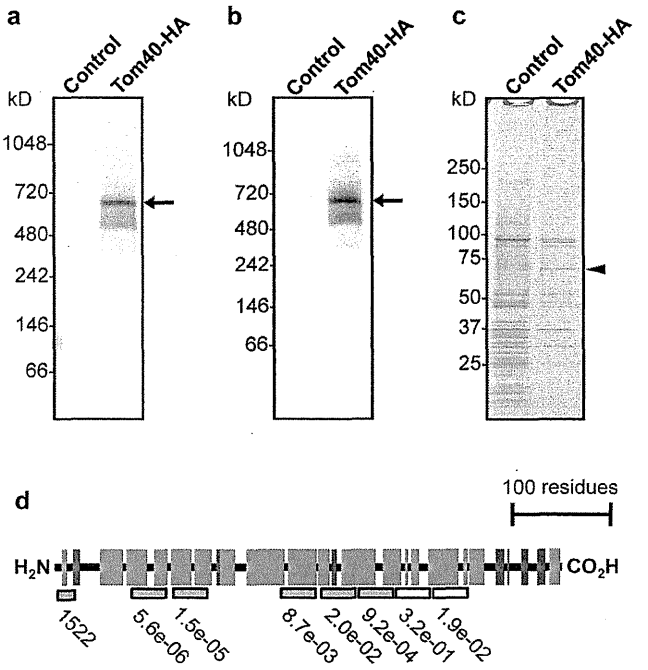

Figure 1 | Identification of the *Entamoeba* TOM complex and its novel subunit. (a), The TOM complex demonstrated by BN-PAGE and immunoblot analysis. (b), Immunoprecipitation of the TOM complex (arrows) from Tom40-HA transformant by BN-PAGE and immunoblot analysis with anti-HA antibody. (c), SDS-PAGE and silver stain of immunoprecipitated TOM complex from Tom40-HA. Arrowhead indicates Tom60. (d), Prediction of the secondary structure and the domain organization of EhTom60. Gray box indicates the hydrophobic cluster, while pink and yellow boxes depict putative tetratricopeptide repeats (TPRs) conserved among genus *Entamoeba* or those specific to *E. histolytica*, respectively. Probability and *E*-value are shown (Supplementary Fig. S4). Green and blue boxes indicate α-helices and β-strands, respectively, predicted by PSIPRED (Supplementary Fig. S6).

(Supplementary Fig. S4), whereas they were not identified in bacteria, archaea, and other eukaryotes. Among amoebozoan organisms, we confirmed by BLAST search (using the threshold of *E*-value < 0.1) that a Tom60 homolog is absent in the *Dictyostelium discoideum* (dictyBase: http://dictybase.org/) and *Acanthamoeba catellani* (https://www.hgsc.bcm.edu/content/acanthamoeba-castellani-neff) genomes, and the transcriptome of *Mastigamoeba balamuthi* (Spears, C. and Roger, A., personal communication).

In silico analyses indicate that *Entamoeba* Tom60 contains putative tetratricopeptide repeats (TPRs)[25] and an amino-terminal hydrophobic cluster (Fig. 1d and Supplementary Fig. S4). TPRs are implicated in protein-protein interactions, and are also present in Tom20 and Tom70, which are membrane-spanning receptors for mitochondrial import[26], suggesting that *Entamoeba* Tom60 may be a receptor for mitosomal import. However, in contrast to the above-mentioned TPR-containing mitochondrial receptors, which consist of only α-helices, *Entamoeba* Tom60 appears to contain β-strands, based on the secondary structure prediction by PSIPRED (http://bioinf.cs.ucl.ac.uk/psipred/) (Fig. 1d and Supplementary Fig. S6). The predicted structural differences argue against the premise that *Entamoeba* Tom60 has a common evolutionary origin with Tom20 and Tom70.

Furthermore, phylogenetic analyses of TPR elements from 23 yeast proteins, plant Toc64, human Tom34 (Supplementary Table S2), 36 *D. discoideum* proteins (Supplementary Table S3), and 28 TPR-containing proteins from *Entamoeba* (Supplementary

Table S4), showed that TPRs of *Entamoeba* Tom60s have no significant affinity with TPRs from other proteins. Therefore, we conclude that *Entamoeba* Tom60 is a genus-specific protein.

Localization and membrane topology of Tom60. We confirmed by IFA the mitosomal localization of Tom60 in an *E. histolytica* cell line expressing Tom40-Myc and Tom60-HA. EhTom40, EhTom60, and APS kinase[9] (APSK; XP_656278) were colocalized and concentrated in the mitosomes (Fig. 2a). However, faint cytosolic signals were also detected for EhTom60 (data not shown). Next, to verify localization, cellular fractionation of lysates was performed, followed by immunoblot analysis. EhTom60 was detected in both the 100,000 × *g* organelle fraction and the soluble supernatant fraction, suggesting that EhTom60 is present in both mitosomes and the cytosol. We next investigated the topology of EhTom60, EhTom40, and other mitosomal proteins by examining their sensitivity to proteinase K treatment followed by immunoblot analysis (Fig. 2b). Proteinase K sensitivity increased in the order of APSK-HA, AAC-HA (inner membrane protein[23,27])/Tom40-HA, and Tom60-HA (Fig. 2b). Furthermore, sodium carbonate treatment, which liberates soluble and peripheral membrane proteins from organelles[28], decreased the amount of organelle-associated Tom60-HA and increased that of soluble Tom60-HA, while Tom40-HA and CPBF1-HA (single-membrane spanning protein)[29] remained in the pellet fraction after the treatment (Fig. 2b, left and Fig. 2c). These data demonstrate that EhTom60 is a cytosolic protein which can associate with EhTom40 on the surface of the mitosomal outer membrane.

Phenotypes of *Tom40*- and *Tom60*-gene silencing. The importance of mitosomal matrix proteins, i.e., ATP sulfurylase (AS; XP_653570), APSK, inorganic pyrophosphatase (IPP; XP_649445), Cpn60, and AAC for *E. histolytica* proliferation was previously verified by gene silencing[27]. To demonstrate the biological importance of the mitosomal import machinery per se, we established *E. histolytica* strains in which *EhTom40* and *EhTom60* genes were silenced. Gene silencing was verified by quantitative real-time PCR (Fig. 3a). Repression of *EhTom40* and *EhTom60* genes caused a decrease in the transport of mitosomal matrix proteins, Cpn60,

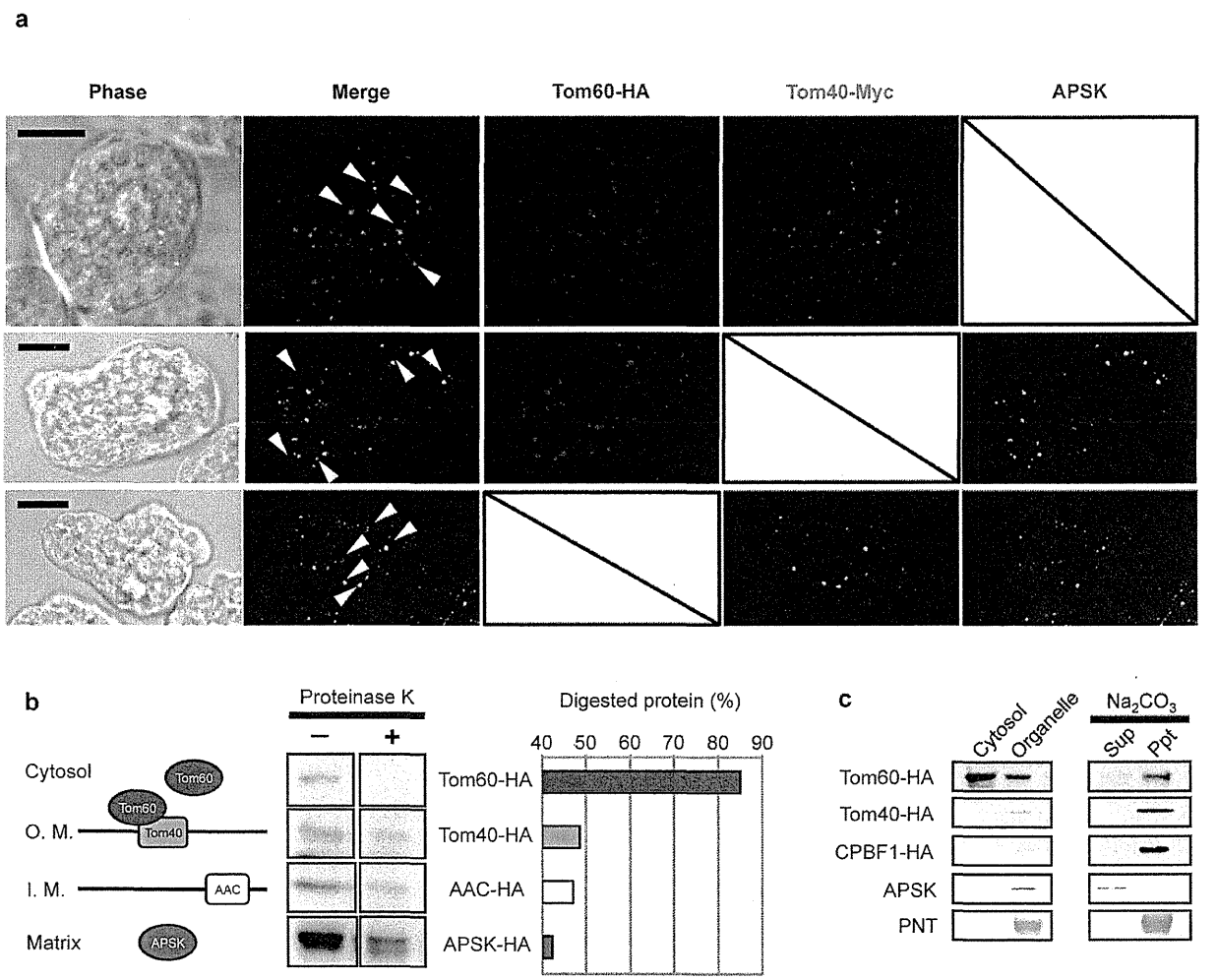

Figure 2 | Localization and topology of Tom40 and Tom60. (a), Indirect fluorescence analyses of Tom40-HA and Tom60-Myc. Anti-APSK antiserum was used as mitosomal marker. Scale bar = 10 μm. (b), Differential sensitivity of several mitosomal proteins to proteinase K treatment. Left panel shows expected topologies of Tom60, Tom40, AAC, and APSK. "O. M." and "I. M." indicate outer and inner membranes, respectively. Middle panel shows immunoblots of each organelle fraction treated (+) or untreated (−) with proteinase K. Right panel shows the ratio of digested protein to that of total undigested protein. (c), Fractionation of mitosomal components. Lysates from amoebae expressing Tom60-HA, Tom40-HA, and CPBF1 (cysteine protease binding family protein 1; XP_655218[29])-HA were fractionated. The three upper and two lower blots were reacted with anti-HA, anti-APSK, or anti-pyridine nucleotide transhydrogenase (PNT, XP_001914099[55]) antibody. CPBF1 and PNT serve as a control for single- and multi-membrane spanning proteins, respectively.

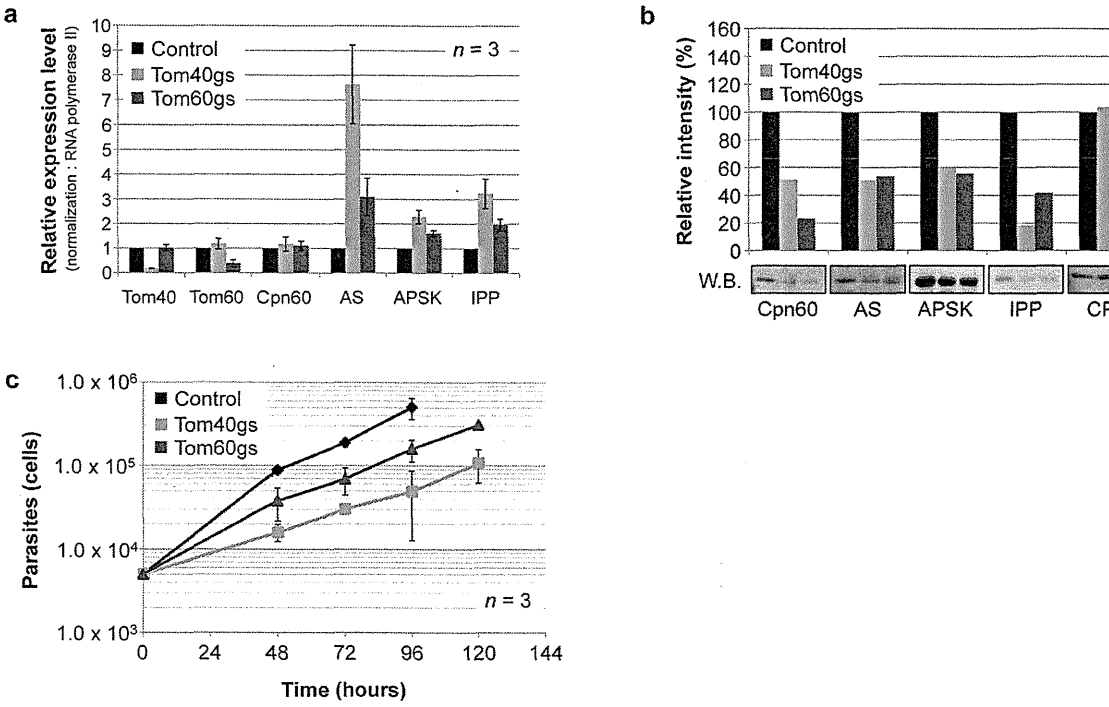

Figure 3 | Phenotypes of *Tom40*- and *Tom60*-gene silenced strain. (a), Effects on the relative mRNA expression levels of mitosomal proteins of *Tom40*- and *Tom60*-gene silencing. Error bars indicate standard deviations. (b), Effects on the amount of mitosomal proteins in organelle fractions from *Tom40*-gene silenced (gs) and Tom60gs strains. Cysteine protease 5 (CP5) was used as loading control. Relative levels of each transcript and protein are shown after normalization against control. (c), Growth kinetics of Tom40gs, Tom60gs, and control strains.

AS, APSK, and IPP (Fig. 3b). On the contrary, we observed a remarkable accumulation of AS, APSK, and IPP transcripts in *EhTom40*- and *EhTom60*-gene silenced strains (Fig. 3a). Finally, repression of *EhTom40* and *EhTom60* genes caused growth retardation when compared to control (Fig. 3c), suggesting that EhTom40 and EhTom60 are important for proliferation. These data also suggest that gene transcription of matrix proteins was upregulated by compensatory mechanisms, but was not sufficient to overcome undesirable effects caused by the repression of proteins involved in the mitosome import. Taken together, we conclude that EhTom40 and EhTom60 play essential roles in the import of matrix proteins to mitosomes.

Tom60 serves as a cytosolic receptor of mitosomal proteins. To verify whether EhTom60 functions as a receptor subunit of the TOM complex, we performed an *in vitro* binding assay, using recombinant AS and cysteine synthase isotype 3 (CS3, XP_653246; control for an irrelevant cytosolic protein) that have the FLAG-tag at the carboxyl terminus, and recombinant His-Tom60ΔN-HA, which lacks the amino-terminal hydrophobic region (a.a. 1–30) of EhTom60, and contained the His-tag at the amino terminus. We removed the amino-terminal region of EhTom60 because it negatively affected solubility of the recombinant protein. His-Tom60ΔN-HA showed a higher binding affinity towards AS-FLAG than CS3-FLAG (Fig. 4a and b; Supplementary Fig. S7). Moreover, the binding efficiency of His-Tom60ΔN-HA to AS-FLAG, but not CS3-FLAG, increased at higher KCl concentrations, which agreed well with the salt dependence of the binding between mitochondrial preproteins and the yeast Tom20[30]. These results strongly suggest that EhTom60 functions as a receptor for soluble proteins imported into the mitosomal matrix.

It has been demonstrated that in fungi, metazoa, and plants, mitochondrial transport of matrix and membrane proteins is mediated by different receptors, Tom20 and Tom70, respectively. Tom20 directly recognizes the amino-terminal presequence of soluble matrix proteins. However, Tom70 interacts with membrane preproteins directly, or indirectly via cytosolic heat shock protein 70 (Hsp70) and Hsp90 chaperones. In the latter case, Hsp70 and Hsp90 that are bound to mitochondrial membrane preproteins[31] further bind to the TPR domains of Tom70 via their conserved tetrapeptide "EEVD" motif at the carboxyl terminus[32]. We thus tested if *Entamoeba* TPR-containing Tom60 can also recognize the tetrapeptide motif present in *E. histoltyica* Hsp70 and Hsp90. His-Tom60ΔN-HA was mixed with recombinant CS3-FLAG or its engineered form (CS3-FLAG-EEVD), which has the tetrapeptide motif at the carboxyl terminus. CS3-FLAG-EEVD, but not CS-FLAG, efficiently bound to His-Tom60ΔN-HA (Fig. 4c). These results indicate that the EhTom60 is involved in the mitosomal transport of membrane proteins via cytosolic Hsp70 and Hsp90.

Discussion

We have demonstrated that *Entamoeba* possesses Tom60, a novel genus-specific peripheral membrane component of the TOM complex, that functions as a receptor/carrier to transport mitosomal proteins from the cytoplasm to mitosomes. One of the striking features of Tom60 is its bipartite localization, which allows Tom60 to function as a carrier of *de novo* synthesized mitosomal preproteins in the cytoplasm and a structural component of the TOM complex on the mitosomal membrane. In this respect, *Entamoeba* Tom60 resembles a mammalian peripheral membrane protein, Tom34, which serves as a co-chaperone of Hsp70 and Hsp90 in a Tom70-dependent transport[33]. However, there is a clear difference between *Entamoeba* Tom60 and mammalian Tom34. Tom60 has direct physical interaction with TOM complex, whereas Tom34 is indirectly associated with Tom40 via Tom22 and Tom70[33,34]. Moreover, *Entamoeba* Tom60 appears to play an indispensable role, judged from the severe growth defect caused by gene silencing (knock down), similar to yeast Tom20 and Tom70[35], whereas Tom34-deficient mice were

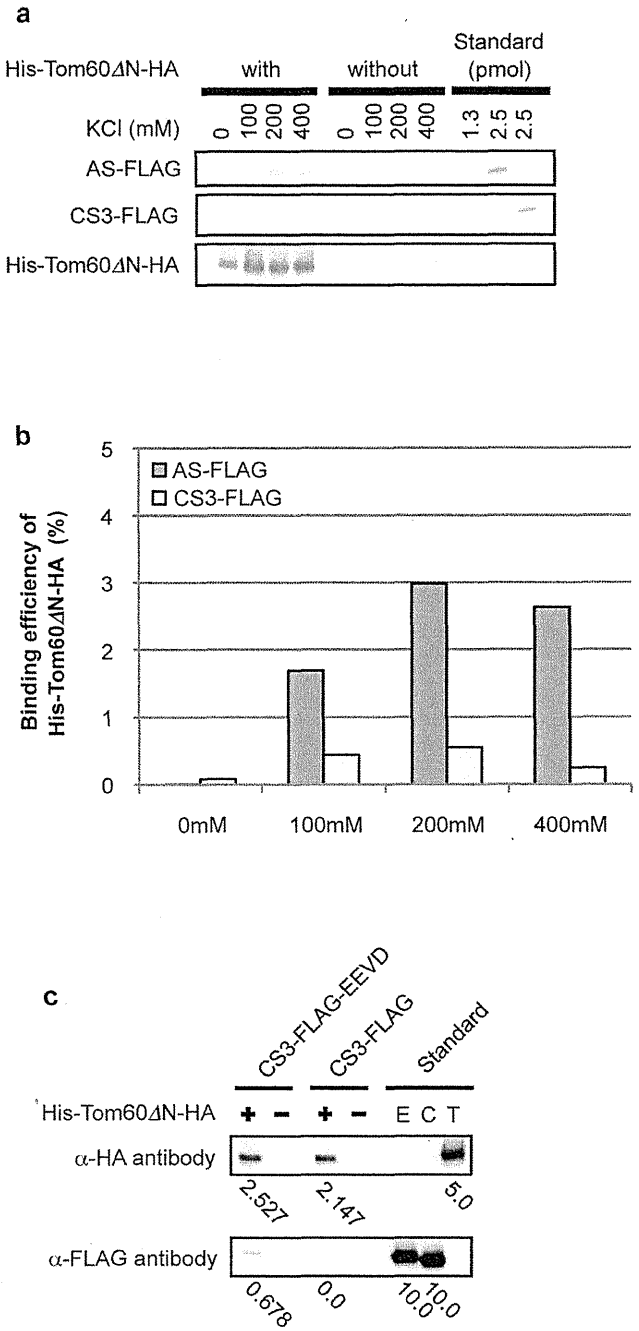

Figure 4 | *In vitro* binding assay of Tom60 and a mitosomal protein. (a), Immunoblotting of proteins bound to His-Tom60ΔN-HA. AS-FLAG is a mitosomal matrix protein, while CS3-FLAG is a cytosolic protein as a control. Approximately 40% of the whole eluates and 1.3 or 2.5% of standards used for the binding assay were subjected to SDS-PAGE and immunoblot analyses with anti-HA and anti-FLAG mouse monoclonal antibody (clone M2, Sigma-Aldrich Japan). (b), Relative binding efficiency of His-Tom60ΔN-HA towards a mitosomal matrix protein. The data were quantitated based on the result shown in Fig. 4a. Vertical and horizontal axes indicate the binding efficiency of His-Tom60ΔN-HA towards substrates and the KCl concentrations, respectively. Low bars in the graph are described numerically while measurements and calculations are described in Supplementary Fig. S7 and Supplementary Methods. (c), The verification of interaction between His-Tom60ΔN-HA and the "EEVD" motif. CS3-FLAG-EEVD is an engineered cytosolic protein in which the "EEVD" motif was added to the carboxyl terminus, like in cytosolic Hsp70 and Hsp90, while CS3-FLAG is a negative control. Approximately 50% of the whole eluates and 5.0 or 10.0 pmol of standards used for the binding assay were subjected to SDS-PAGE and immunoblot analysis, as described above. "E", "C", and "T" stand for CS3-FLAG-EEVD, CS3-FLAG, and His-Tom60ΔN-HA, respectively. Values below panels indicate protein amounts (pmol) estimated by densitometric scanning of the blots.

viable, grew normally, and had a normal Mendelian inheritance pattern[36]. Thus, *Entamoeba* Tom60 represents an unprecedented essential bipartite-localized receptor/carrier for the protein import to MROs. It was presumed that Tom20 and Tom70 are loosely associated with other components of TOM complex, mobilized on the entire mitochondrial surface, and capable of interacting with preproteins[37]. Similarly, we assume that cytosolic localization of the *Entamoeba* Tom60 also maximizes the chance of its interaction with mitosomal preproteins. The mechanisms of the recruitment of Tom60 to the mitosomal outer membrane remain unsolved. One possibility is that Tom60 loaded with a precursor protein docks to the TOM complex, whereas free unloaded Tom60 remains dissociated from the TOM complex in the cytosol. Another possibility is the post-translational modifications. It has been recently reported that the binding of mammalian Tom20 and Tom70 toward preproteins is regulated by phosphorylation[38].

Tom60 is a robust receptor for the mitosomal transport. Tom60 seems to transport both soluble and membrane mitosomal proteins. It has been shown in Opisthokonta that mitochondrial soluble matrix and membrane preproteins are transported via binding with distinct TPR-containing mitochondrial receptors, namely Tom20 and Tom70, which recognizes the amino-terminal transit peptide or the internal (cryptic) targeting signals, respectively[31]. Subsequently, these preproteins are passed from Tom20 and Tom70 to Tom22 and inserted into the Tom40 channel[31]. Therefore, Tom22 plays a role as a receptor for both mitochondrial soluble matrix and membrane preproteins. Similarly, *Entamoeba* Tom60 binds to a soluble mitosomal matrix protein, AS, as well as the "EEVD" motif, which is conserved in cytosolic Hsp70 and Hsp90 from three *Entamoeba* species. It was demonstrated that in mammals, cytosolic Hsp70 and Hsp90 are involved in the Tom70-dependent transport of mitochondrial membrane preproteins to TOM complex[39]. Among MRO-containing eukaryotes, no organism that possesses both Tom70 and Tom20 has been discovered. *Encephalitozoon*[1] and *Blastocystis*[40,41] encodes only a Tom70 homolog, suggesting that the Tom70 homolog may play a bifunctional role similar to *Entamoeba* Tom60. In contrast, in *Giardia*[42], *Trichomonas*[43], and *Cryptosporidium*[44], no potential receptor component of TOM complex has been identified. These organisms most likely possess a lineage-specific receptor like *Entamoeba* Tom60. Further investigation is needed to clarify if such lineage-specific functional Tom60 homologs also contain the TPR domains for the cargo interaction.

It was hypothesized that the TOM complex in early eukaryotes is composed of Tom40, Tom22, and Tom7[17]. It was also shown that the TOM complex of the aerobic free-living social amoebozoan *D. discoideum* consists of Tom40, Tom22, Tom7, and Tom6, and lacks Tom20 and Tom70[7,13]. These data indicate that a common ancestor of amoebozoan species also contained Tom40, Tom22, and Tom7 in its TOM complex. This presumption is also supported by the existence of Tom40 homologs in the genome of other amoebozoan species including *Polysphondylium*[45], and *Acanthamoeba*[45], and the transcriptome of *Mastigamoeba* (Stairs, C. and Roger, A., personal communication), and Tom7 homologs in *Polysphondylium* (EFA78398) and *Acanthamoeba* (Contig6955 in the *Acanthamoeba* genome database). However, we did not detect Tom22 homologs in these amoebozoa. These data are consistent with the premise that *Entamoeba* probably secondarily has lost Tom22 during separation within Amoebozoa. A key question regarding a lineage-specific presence of Tom60 in *Entamoeba* is why and how the loss of the

canonical subunit Tom22 and gain of Tom60 occurred. We presume that it is related to the lack of mitosomal targeting sequences in *Entamoeba*[9]. In the general model of mitochondrial matrix protein import, Tom22 interacts with the positive-charged surface in the amphiphilic α-helix of presequences[30,46]. In contrast, such ionic interaction does not appear to mediate the binding between *Entamoeba* Tom60 and mitosomal proteins. An alternative explanation of the loss of Tom22 is that in the *Entamoeba* ancestor the mitosomal proteins that were acquired by lateral gene transfer, such as sulfate activation enzymes, were poorly imported into mitosomes by Tom22.

Our current hypothesis as to how a novel TOM complex evolved in *Entamoeba* mitosomes is as follows: The *Entamoeba* ancestor was exposed to anaerobic environments, under which oxygen-dependent energy generation became unusable. Under these conditions, the mitochondrion lost its electron transport chain, membrane potential, and other aerobic mitochondrion-related functions. The loss of membrane potential across the inner membrane promoted an elimination of the canonical membrane potential-dependent TIM23 and TIM22 complexes[31]. In agreement with this hypothesis, membrane potential-dependent AAC, that is present in the aerobic mitochondria, became non-reliant on the membrane potential in *E. histolytica*[23]. Moreover, as described above, *Entamoeba* mitosomal proteins lack a canonical positively-charged transit peptide[9], which is utilized for the electrophoretic import via the membrane potential[31]. Alterations of the TIM complex led to the rearrangement of the TOM complex, more specifically loss of Tom22, which is associated with the TIM23 complex in a typical aerobic mitochondrion. Finally, loss of Tom22 must have been compensated with the invention of a new targeting mechanism dependent on Tom60. It was also suggested that subunit replacement might have occurred in the TIM complex of *Trichomonas vaginalis*[43] and *Giardia intestinalis*[42]. It is worth further investigating how commonly replacement of subunits occurred in anaerobic MRO-possessing eukaryotes.

Methods

Organisms. Trophozoites of *Entamoeba histolytica* HM-1:IMSS cl6[47] and G3[48] strains were cultivated axenically in Diamond BI-S-33 medium[49].

RNA and cDNA preparation. Total RNA was isolated from various strains by TRIZOL® reagent (Invitrogen, Carlsbad, San Diego, CA). mRNA was purified using GenElute™ mRNA Miniprep Kits (Sigma-Aldrich Japan). cDNA was synthesized from mRNA using SuperScript™ III RNase H⁻ reverse transcriptase (Invitrogen), oligo(dT)$_{20}$ primer, and primer 1 (Supplementary Table S5).

Plasmid construction. *E. histolytica Tom40* and *Tom60* genes were PCR-amplified from cDNA using Phusion DNA polymerase (New England Biolabs, Beverly, MA) and corresponding primer sets (Supplementary Table S5). After restriction digestion, amplified fragments were ligated into pEhEx/HA[50] and pEhEx/Myc[29] using Ligation-Convenience Kit (Nippongene, Tokyo, Japan). To generate the plasmid for Tom40-Myc/Tom60-HA double-expression, a fragment containing the Tom40-Myc protein coding region flanked by the upstream and downstream regions of the *CS1* gene was PCR-amplified from pEhEx/Tom40-Myc by primers 6/7 (Supplementary Table S5), and inserted into the *Spe* I-digested pEhEx/Tom60-HA using In-Fusion® system (TaKaRa, Shiga, Japan). For gene silencing, a 400-bp fragment corresponding to the amino terminus of Tom40 and Tom60 was PCR-amplified with appropriate primers (Supplementary Table S5). Restriction-digested fragments were ligated into *Stu* I/*Sac* I double-digested psAP-2-Gunma plasmid[27].

Amoeba transformation. Lipofection of trophozoites, selection, and maintenance of transformants were performed as previously described[9].

Immunofluorescence assay. IFA[9,51] was performed as previously described.

Preparation of organelle fraction. Amoeba strains that expressed HA-tagged Tom60-HA, Tom40-HA, AAC-HA, APSK-HA, and CPBF1-HA[29] proteins, strains in which *Tom40* and *Tom60* genes were silenced, and mock transformants (pEhEx/HA and psAP2-Gunma) were washed three times with 2% glucose/PBS. After resuspension in lysis buffer (10 mM MOPS-KOH, pH7.2, 250 mM sucrose, protease inhibitors), cells were disrupted mechanically by a Dounce homogenizer. Unbroken cells were removed by centrifugation at 5,000 × *g* for 10 min, and the supernatant centrifuged at 100,000 × *g* for 60 min to separate the organelle and cytosolic fractions. The 100,000 × *g* organelle fractions were resuspended with lysis buffer, and were recollected by the centrifugation at 100,000 × *g* for 60 min.

Immunoprecipitation of the TOM complex. Organelle fractions were solubilized with IP buffer (2% digitonin/50 mM BisTris-HCl, pH7.2/50 mM NaCl/10% [W/V] glycerol, protease inhibitors). The lysate was mixed with Protein G-Sepharose 4 Fast Flow (GE Healthcare), and Sepharose beads were removed by centrifugation. Precleared lysates were mixed with anti-HA mouse monoclonal antibody conjugated with agarose (Sigma-Aldrich Japan) at 4°C for 3 h. Agarose was washed three times with IP buffer containing 1% digitonin. Bound protein was eluted by IP buffer containing 1% digitonin and 600 μg/ml HA peptide (Sigma-Aldrich Japan).

Blue native polyacrylamide gel electrophoresis (BN-PAGE). Organelle fractions were solubilized by either 2% digitonin or n-dodecyl-β-D-maltoside (DDM) at 4°C for 30 min, and centrifuged at 20,000 × *g* for 30 min at 4°C. BN-PAGE was performed using NativePAGE™ Novex® Bis-Tris Gel System (Invitrogen) according to manufacturer's protocol. Immunoprecipitated samples were mixed with 0.25% Coomassie® G-250 (Invitrogen) before electrophoresis.

Liquid chromatography-tandem mass spectrometric analysis. In-gel trypsin digestion of protein bands of interest and LC-MS/MS were performed as previously described[52,53].

Proteinase K treatment. Organelle fractions (50 μg protein each) were treated with or without final 2.8 μg/ml proteinase K (Roche) at 4°C for 15 min, followed by SDS-PAGE and immunoblot analysis with anti-HA mouse monoclonal antibody. Band intensities were evaluated using the Analysis Toolbox in ImageQuant TL software (GE Healthcare).

Na_2CO_3 treatment. Organelle fractions (1 mg protein) in lysis buffer were diluted 20 times with ice-cold 100 mM Na_2CO_3, pH 11.5 and 150 mM NaCl, kept at 4°C for 30 min, and centrifuged at 100,000 × *g* for 60 min. The 100,000 × *g* supernatant was transferred to a fresh tube and the precipitate washed once with Na_2CO_3 solution. Immunoblot analysis was performed as described above. Anti-PNT (1 : 1,000) and anti-APSK (1 : 1,000) rabbit antisera were used as primary antibodies. Alkaline phosphatase-conjugated anti-rabbit IgG antibody (Jackson ImmunoResearch, West Grove, PA) was used as secondary antibody.

Quantitative real-time PCR. Quantitative real-time PCR analysis was performed as described[27] using primer sets (primers 12-25; Supplementary Table S5) for *Tom40*, *Tom60*, *Cpn60*, *AS*, *APSK*, *IPP*, and *Rnapol* (XM_643999) genes.

Recombinant proteins. To generate recombinant histidine tagged (His_6)-Tom60ΔN-HA, AS-FLAG, CS3-FLAG, and CS3-FLAG-EEVD proteins, we amplified *Tom60*, *AS*, and *CS3* genes using appropriate primers sets (Supplementary Table S5) and pEhEx/Tom60-HA, pEhEx/AS-HA[9], and pET15b/CS3[54] as templates. Fragments were digested by appropriate sets of restriction enzymes and ligated into pCold I (TaKaRa). These plasmids were transformed into BL21 Star™(DE3) One Shot® Chemically Competent *E. coli* (Invitrogen) and expression of recombinant proteins was induced by 1 mM IPTG. After lysis of bacteria and purification by Ni-NTA system (QIAGEN GmbH, Hilden, Germany), the His_6-tag was removed from His_6-AS-FLAG, His_6-CS-FLAG and His_6-CS-FLAG-EEVD by AcTEV™ protease (Invitrogen).

***In vitro* binding assay of Tom60.** The binding efficiency of His_6-Tom60ΔN-HA was calculated and shown as the ratio of eluted AS-FLAG or CS3-FLAG to that of eluted His-Tom60ΔN-HA in the *in vitro* binding assay (Supplementary Methods). The hydrophobic nature of the amino terminus of Tom60 negatively affected solubility, thus it was removed prior to the binding assay. To verify the interaction between His_6-Tom60ΔN-HA and the "EEVD" motif, we carried out the assay with CS3-FLAG-EEVD or CS3-FLAG. Assay condition was identical to *in vitro* binding assay as described in Supplementary Methods except that the assay buffer contained 50 mM KCl.

1. Lill, R. & Kispal, G. Maturation of cellular Fe-S proteins: an essential function of mitochondria. *Trends Biochem Sci.* **8**, 352–356 (2000).
2. Maralikova, B. *et al.* Bacterial-type oxygen detoxification and iron-sulfur cluster assembly in amoebal relict mitochondria. *Cell Microbiol.* **3**, 331–342 (2010).
3. Tovar, J. *et al.* Mitochondrial remnant organelles of *Giardia* function in iron-sulphur protein maturation. *Nature.* **426**, 172–176 (2003).
4. Sutak, R. *et al.* Mitochondrial-type assembly of FeS centers in the hydrogenosomes of the amitochondriate eukaryote *Trichomonas vaginalis*. *Proc Natl Acad Sci U S A.* **101**, 10368–10373 (2004).
5. Goldberg, A. V. *et al.* Localization and functionality of microsporidian iron-sulphur cluster assembly proteins. *Nature.* **452**, 624–628 (2008).
6. Tsaousis, A. D. *et al.* Evolution of Fe/S cluster biogenesis in the anaerobic parasite *Blastocystis*. *Proc Natl Acad Sci U S A.* **109**, 10426–10431 (2012).
7. Lithgow, T. & Schneider, A. Evolution of macromolecular import pathways in mitochondria, hydrogenosomes and mitosomes. *Philos Trans R Soc Lond B Biol Sci.* **365**, 799–817 (2010).
8. Heinz, E. & Lithgow, T. Back to basics: A revealing secondary reduction of the mitochondrial protein import pathway in diverse intracellular parasites. *Biochim Biophys Acta.* In press (2012).

9. Mi-ichi, F., Yousuf, M. A., Nakada-Tsukui, K. & Nozaki, T. Mitosomes in *Entamoeba histolytica* contain a sulfate activation pathway. *Proc Natl Acad Sci USA.* **106**, 21731–21736 (2009).
10. Dagley, M. J. *et al.* The protein import channel in the outer mitosomal membrane of *Giardia intestinalis*. *Mol Biol Evol.* **9**, 1941–1947 (2009).
11. Dyall, S. D. *et al. Trichomonas vaginalis* Hmp35, a putative pore-forming hydrogenosomal membrane protein, can form a complex in yeast mitochondria. *J Biol Chem* **278**, 30548–30561 (2003).
12. Shiflett, A. M. & Johnson, P. J. Mitochondrion-related organelles in eukaryotic protists. *Annu Rev Microbiol.* **64**, 409–429 (2010).
13. Dolezal, P. *et al.* The essentials of protein import in the degenerate mitochondrion of *Entamoeba histolytica*. *PLoS Pathog.* **6**, e1000812 (2010).
14. Dolezal, P., Likic, V., Tachezy, J. & Lithgow, T. Evolution of the molecular machines for protein import into mitochondria. *Science.* **313**, 314–318 (2006).
15. Hoogenraad, N. J., Ward, L. A. & Ryan, M. T. Import and assembly of proteins into mitochondria of mammalian cells. *Biochim Biophys Acta.* **1592**, 97–105 (2002).
16. Pfanner, N., Wiedemann, N., Meisinger, C. & Lithgow, T. Assembling the mitochondrial outer membrane. *Nat Struct Mol Biol.* **11**, 1044–1048 (2004).
17. Maćasev, D. *et al.* Tom22', an 8-kDa trans-site receptor in plants and protozoans, is a conserved feature of the TOM complex that appeared early in the evolution of eukaryotes. *Mol Biol Evol.* **8**, 1557–1564 (2004).
18. Chew, O. *et al.* A plant outer mitochondrial membrane protein with high amino acid sequence identity to a chloroplast protein import receptor. *FEBS Lett.* **557**, 109–114 (2004).
19. Pusnik, M. *et al.* Mitochondrial preprotein translocase of trypanosomatids has a bacterial origin. *Curr Biol.* **21**, 1738–1743 (2011).
20. Perry, A. J., Hulett, J. M., Likić, V. A., Lithgow, T. & Gooley, P. R. Convergent evolution of receptors for protein import into mitochondria. *Curr Biol.* **16**, 221–229 (2006).
21. Stanley, S. L. Jr. Amoebiasis. *Lancet.* **361**, 1025–1034 (2003).
22. León-Avila, G. & Tovar, J. Mitosomes of *Entamoeba histolytica* are abundant mitochondrion-related remnant organelles that lack a detectable organellar genome. *Microbiology.* **150**, 1245–1250 (2004).
23. Chan, K. W. *et al.* A novel ADP/ATP transporter in the mitosome of the microaerophilic human parasite *Entamoeba histolytica*. *Curr Biol.* **15**, 737–742 (2005).
24. Model, K. *et al.* Multistep assembly of the protein import channel of the mitochondrial outer membrane. *Nat Struct Biol.* **8**, 361–370 (2001).
25. Karpenahalli, M. R., Lupas, A. N. & Söding, J. TPRpred: a tool for prediction of TPR-, PPR- and SEL1-like repeats from protein sequences. *BMC Bioinformatics.* **8**, 2. (2007).
26. Baker, M. J., Frazier, A. E., Gulbis, J. M. & Ryan, M. T. Mitochondrial protein-import machinery: correlating structure with function. *Trends Cell Biol.* **17**, 456–464 (2007).
27. Mi-ichi, F. *et al.* Sulfate activation in mitosomes plays an important role in the proliferation of *Entamoeba histolytica*. *PLoS Negl Trop Dis.* **5**, e1263 (2011).
28. Fujiki, Y. *et al.* Polypeptide and phospholipid composition of the membrane of rat liver peroxisomes: comparison with endoplasmic reticulum and mitochondrial membranes. *J Cell Biol.* **93**, 103–110 (1982).
29. Nakada-Tsukui, K. *et al.* A novel class of cysteine protease receptors that mediate lysosomal transport. *Cell Microbiol.* **14**, 1299–1317 (2012).
30. Brix, J., Dietmeier, K. & Pfanner, N. Differential recognition of preproteins by the purified cytosolic domains of the mitochondrial import receptors Tom20, Tom22, and Tom70. *J. Biol. Chem.* **272**, 20730–20735 (1997).
31. Chacinska, A. *et al.* Importing mitochondrial proteins: machineries and mechanisms. *Cell.* **138**, 628–644 (2009).
32. Young, J. C., Hoogenraad, N. J. & Hartl, F. U. Molecular chaperones Hsp90 and Hsp70 deliver preproteins to the mitochondrial import receptor Tom70. *Cell.* **112**, 41–50 (2003).
33. Faou, P. & Hoogenraad, N. J. Tom34: a cytosolic cochaperone of the Hsp90/Hsp70 protein complex involved in mitochondrial protein import. *Biochim Biophys Acta.* **1823**, 348–357 (2012).
34. van Wilpe, S. *et al.* Tom22 is a multifunctional organizer of the mitochondrial preprotein translocase. *Nature.* **401**, 485–489 (1999).
35. Moczko, M. *et al.* Deletion of the receptor MOM19 strongly impairs import of cleavable preproteins into *Saccharomyces cerevisiae* mitochondria. *J Biol Chem.* **269**, 9045–9051 (1994).
36. Terada, K. *et al.* Expression of Tom34 splicing isoforms in mouse testis and knockout of Tom34 in mice. *J Biochem.* **133**, 625–631 (2003).
37. Dekker, P. J. *et al.* Preprotein translocase of the outer mitochondrial membrane: Molecular dissection and assembly of the general import pore complex. *Mol Cell Biol.* **18**, 6515–6524 (1998).
38. Schmidt, O. *et al.* Regulation of mitochondrial protein import by cytosolic kinases. *Cell.* **144**, 227–239 (2011).
39. Young, J. C., Hoogenraad, N. J. & Hartl, F. U. Molecular chaperones Hsp90 and Hsp70 deliver preproteins to the mitochondrial import receptor Tom70. *Cell.* **112**, 41–50 (2003).
40. Denoeud, F. *et al.* Genome sequence of the stramenopile *Blastocystis*, a human anaerobic parasite. *Genome Biol.* **12**, R29 (2011).
41. Tsaousis, A. D. *et al.* A functional Tom70 in the human parasite *Blastocystis* sp.: implications for the evolution of the mitochondrial import apparatus. *Mol Biol Evol.* **28**, 781–791 (2011).
42. Jedelský, P. L. *et al.* The minimal proteome in the reduced mitochondrion of the parasitic protist *Giardia intestinalis*. *PLoS One.* **6**, e17285 (2011).
43. Rada, P. *et al.* The core components of organelle biogenesis and membrane transport in the hydrogenosomes of *Trichomonas vaginalis*. *PLoS One.* **6**, e24428 (2011).
44. Alcock, F. *et al.* A small Tim homohexamer in the relict mitochondrion of *Cryptosporidium*. *Mol Biol Evol.* **29**, 113–122 (2012).
45. Wojtkowska, M. *et al.* Phylogenetic analysis of mitochondrial outer membrane β-barrel channels. *Genome Biol Evol.* **4**, 110–125 (2012).
46. Yamano, K. *et al.* Tom20 and Tom22 share the common signal recognition pathway in mitochondrial protein import. *J Biol Chem.* **283**, 3799–3807 (2008).
47. Diamond, L. S., Mattern, C. F. & Bartgis, I. L. Viruses of *Entamoeba histolytica*. I. Identification of transmissible virus-like agents. *J Virol.* **9**, 326–341 (1972).
48. Bracha, R., Nuchamowitz, Y., Anbar, M. & Mirelman, D. Transcriptional silencing of multiple genes in trophozoites of *Entamoeba histolytica*. *PLoS Pathog.* **2**, e48 (2006).
49. Diamond, L. S., Harlow, D. R. & Cunnick, C. C. A new medium for the axenic cultivation of *Entamoeba histolytica* and other. *Entamoeba. Trans R Soc Trop Med Hyg* **72**, 431–432 (1978).
50. Nakada-Tsukui, K., Okada, H., Mitra, B. N. & Nozaki, T. Phosphatidylinositol-phosphates mediate cytoskeletal reorganization during phagocytosis via a unique modular protein consisting of RhoGEF/DH and FYVE domains in the parasitic protozoon *Entamoeba histolytica*. *Cell Microbiol.* **11**, 1471–1491 (2009).
51. Nakada-Tsukui, K., Saito-Nakano, Y., Ali, V. & Nozaki, T. A Retromerlike Complex Is a Novel Rab7 Effector That Is Involved in the Transport of the Virulence Factor Cysteine Protease in the Enteric Protozoan Parasite *Entamoeba histolytica*. *Mol Biol Cell.* **16**, 5294–5303 (2005).
52. Mineki, R. *et al. In situ* alkylation with acrylamide for identification of cysteinyl residues in proteins during one- and two-dimensional sodium dodecyl sulphate-polyacrylamide gel electrophoresis. *Proteomics.* **2**, 1672–1681 (2002).
53. Makiuchi, T. *et al.* Compartmentalization of a glycolytic enzyme in Diplonema, a non-kinetoplastid euglenozoan. *Protist.* **162**, 482–489 (2011).
54. Husain, A. *et al.* Metabolome Analysis Revealed Increase in *S*-Methylcysteine and Phosphatidylisopropanolamine Synthesis upon l-Cysteine Deprivation in the Anaerobic Protozoan Parasite *Entamoeba histolytica*. *J Biol Chem.* **285**, 39160–39170 (2010).
55. Yousuf, M. A., Mi-ichi, F., Nakada-Tsukui, K. & Nozaki, T. Localization and targeting of an unusual pyridine nucleotide transhydrogenase in *Entamoeba histolytica*. *Eukaryot Cell.* **9**, 926–933 (2010).

Acknowledgments

We thank Tsutomu Fujimura, Reiko Mineki, and Hikari Taka, the Division of Proteomics and Biomolecular Science, Biomedical Research Center at Juntendo University Graduate School of Medicine for mass-spectrometric analysis, Courtney Spears and Andrew J. Roger, Centre for Comparative Genomics and Evolutionary Bioinformatics, Department of Biochemistry and Molecular Biology at Dalhousie University for the information on *Mastigamoeba* transcriptome, Ghulam Jeelani and Eiko Nakasone for technical assistance, and Gil M. Penuliar and Herbert Santos for proof reading. This work was supported by a Grant-in-Aid for Scientific Research from the Ministry of Education, Culture, Sports, Science and Technology (MEXT) of Japan to T.N. (23117001, 23117005, 23390099), a Grant-in-Aid on Bilateral Programs of Joint Research Projects and Seminars from Japan Society for the Promotion of Science, a Grant-in-Aid on Strategic International Research Cooperative Program from Japan Science and Technology Agency, a grant for research on emerging and re-emerging infectious diseases from the Ministry of Health, Labour and Welfare of Japan (H23-Shinko-ippan-014) to T.N., a grant for research to promote the development of anti-AIDS pharmaceuticals from the Japan Health Sciences Foundation (KHA1101) to T.N., Strategic International Research Cooperative Program from Japan Science and Technology Agency to T.N. and by Global COE Program (Global COE for Human Metabolomic Systems Biology) from MEXT, Japan to T.N.

Author contributions

T.M. did the experiments. T.M. and T.N. wrote the manuscript. T.M., F.M., K.N.-T. and T.N. interpreted the data.

Additional information

Supplementary information accompanies this paper at http://www.nature.com/scientificreports

Competing financial interests: The authors declare no competing financial interests.

How to cite this article: Makiuchi, T., Mi-ichi, F., Nakada-Tsukui, K. & Nozaki, T. Novel TPR-containing subunit of TOM complex functions as cytosolic receptor for *Entamoeba* mitosomal transport. *Sci. Rep.* **3**, 1129; DOI:10.1038/srep01129 (2013).